LA-5065-MS

INFORMAL REPORT

Megagauss Field Applications

A Selection of LASL Internal Reports

los alamos
scientific laboratory
of the University of California
LOS ALAMOS, NEW MEXICO 87544

UNITED STATES
ATOMIC ENERGY COMMISSION
CONTRACT W-7405-ENG. 36

In the interest of prompt distribution, this LAMS report was not edited by the Technical Information staff.

LA-5065-MS
Informal Report
SPECIAL DISTRIBUTION
ISSUED: October 1972

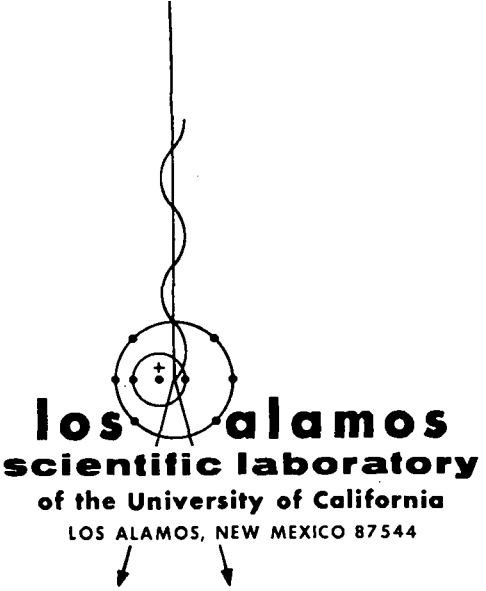

Megagauss Field Applications

A Selection of LASL Internal Reports

Compiled by

C. M. Fowler

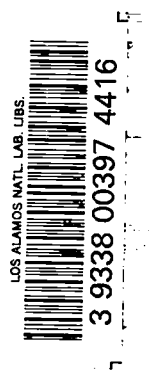

Contributors

R. S. Caird
C. M. Fowler
J. N. Fritz
W. B. Garn
D. B. Thomson

ABSTRACT

This document consists of excerpts taken from LASL internal reports dealing with applications of megagauss magnetic fields. Applications include use of megagauss fields as high-pressure sources, as particle accelerators, and as a medium in which the optical properties of a number of materials are investigated.

TALK

ILWOG MEETING,

Los Alamos Scientific Laboratory

October 21-23, 1970

ILWOG MEETING

Oct. 21-23, 1970

ABSTRACT*

APPROXIMATE ISENTROPIC COMPRESSION BY MAGNETIC FIELDS

C. M. Fowler, R. S. Caird, J. N. Fritz, W. B. Garn and D. B. Thomson

GMX-6, LASL

Magnetic fields can exert pressures on conductors equal to $B^2/8\pi$. Two types of high field systems are described, produced explosively, that are in current use. One system employs cylindrically convergent geometry and produces fields in the range 5-7 megagauss (pressure 1-2 megabars). Much higher fields have been obtained this way but not in a very reproducible manner. If the need is sufficient, this system can probably be extended to 10 megagauss (4 megabars) with reasonable reproducibility. The other system produces fields of 2 MG (150 kbar) in an external load coil of 5/8" i.d. and 3" long; this volume is large enough to house our cryogenic cooling systems. This system is being extended to produce fields in the 3-4 megagauss range (350-600 kbar).

Experimental arrangements in which these fields can be used to compress matter, and techniques for determining the pressure and volume of the sample will be mentioned. Several potential difficulties and some experiments planned to study them will be discussed. Assuming these present no serious obstacles, then the calculations presented in the preceding papers by G. Kerley and J. Barnes suggest that we have a method available to obtain high pressure equation of state data on isentropes to supplement that already available on shock Hugoniots. These data should be particularly interesting for condensed hydrogen species.

*10 minute talk, to follow those of G. Kerley and J. Barnes, T-5, on subject of hydrogen compression.

Approximate Isentropic Compression by Magnetic Fields

C. M. Fowler, R. S. Caird, J. N. Fritz, W. B. Garn and D. B. Thomson

For some time, interest has been expressed in obtaining high pressure equation-of-state data under isentropic conditions. And more recently this is particularly true for hydrogen. For example, starting from the condensed, zero pressure state, three different equation-of-state models predict isentropic compression ratios that range from 3.2 to 5 at 100 kb. Some experimental points in the 50-200 kb range would be useful to resolve these differences. It might be mentioned that single shock compression to 100 kb results in a volume compression ratio of only about 2.4. This is an indication of the increased heating which arises from the nonisentropic shock process.

In view of this interest we have begun an investigation to consider the possibilities of magnetic field compression in cooperation with T-5. The proposed method can be explained with the help of Fig. 1.

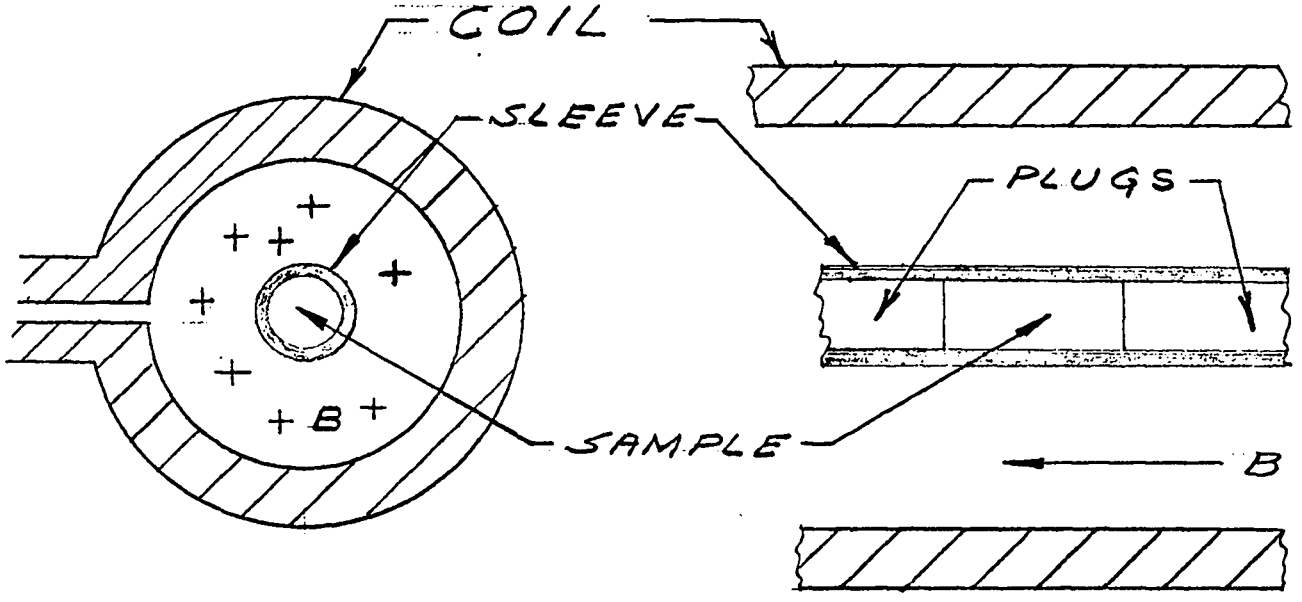

Figure 1

A transient magnetic field, B,is produced in the coil. The sample under study is housed inside a flux-excluding metal sleeve. The magnetic pressure, $B^2/8\pi$, exerted on the sleeve is transmitted to the sample.

There are several explosive flux compression systems available, or under development, that produce large magnetic fields. Their significant properties are given in Table I.

Table I

HE Type	Load	Dia.	L	Peak Field (MG)	~P (kb)	Status
Strip	Ext	5/8"	3"	1.1	50	on hand
Strip (2 stage)	Ext	5/8"	3"	2.	150	on hand
Strip (2 stage)	Ext	5/8"	3"	3-4	350-600	developing
Cylindrical compression	Int	?→1/4"	1"	5-7	1000-2000	on hand
"	Int	?	1"	10	4000	can be dev.

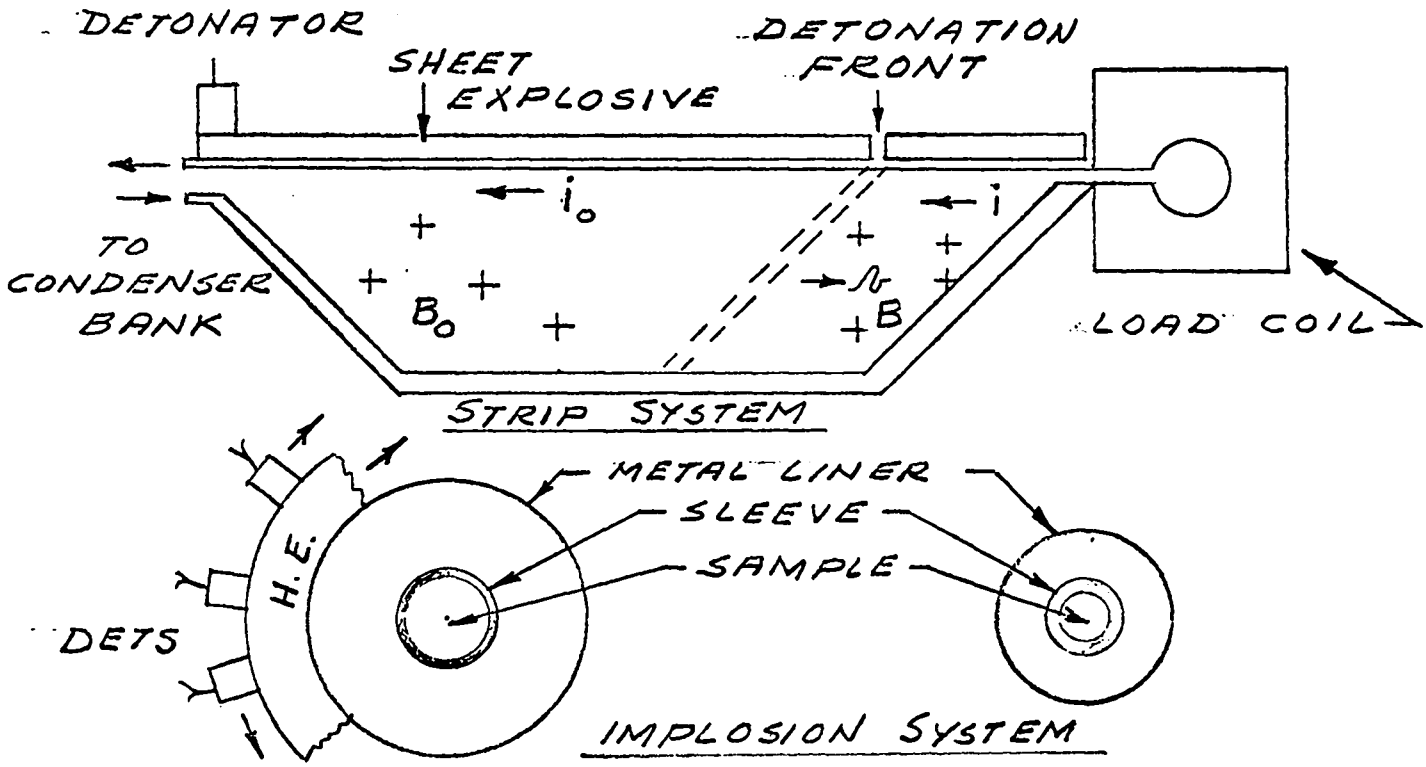

Figure 2

The principles of the two basic systems in use may be seen from Fig. 2. The strip system, which produces fields in the low megagauss range, is shown at the top. Basically, it consists of a metal box with a strip of explosive and detonator, as shown. The load coil is external to the explosively driven part of the system. The metal box is initially open at the input end. Initial flux, supplied by a condenser bank, is put into the circuit consisting of the generator section (box) and load coil. At peak current, after firing the condenser bank, the detonator is triggered. This first shorts the circuit at the input end, thus trapping the flux in the generator and load coil. As the detonation front proceeds down the explosive strip, the upper plate of the generator contacts the bottom plate and drives the flux ahead of the contact surface, thus increasing the field in the load coil. Figure 3 shows the magnetic field and pressure vs time obtained in a two-stage strip system load coil.

The very high fields are obtained in implosion systems by cylindrical compression of a metal cylinder (liner) as shown at the bottom of Fig. 2. Here, initial flux is induced in the liner by means of external coils. At peak flux, the explosive drives the metal liner inward, thus compressing the field. The load region is internal to the system, occupying a small cylindrical region at the center of the liner. The second view of this system shows the system at some later stage of cylindrical compression.

The potential use of the method for equation-of-state techniques rests on the calculations presented in the preceding paper of Kerley and Barnes. Using the drive pressure dependence shown in Fig. 3, they have calculated the dynamic response of a hydrogen sample housed as in Fig. 1. They found the following results:

i) After initial transient distrubances have died down, the pressure and density at later stages in the compression were quite uniform across the radius.

ii) This uniform pressure across the radius of the sample was the same as the instantaneous magnetic drive pressure.

iii) Entropy increase during the compression was not detectable.

They observed similar results with much greater magnetic drive pressures, characteristic of those we obtain in our implosion systems, although some small but calculable nonisentropic heating effects were observed. K. J. Ewing, formerly of GMX-3, obtained similar results two or three years ago, but the results were more qualitative.

We propose to obtain equation-of-state points from these systems as follows:

i) Determine the pressure by measuring the magnetic field.

ii) Determine the volume by flash x-radiography, aided by measurements of additional flux picked up by a loop surrounding the metal sleeve as it compresses.

This procedure is similar to the well-established shock wave technique where p and v are inferred from shock and particle velocity. Here, however, the state locus is assumed to be on an isentrope instead of the shock Hugoniot.

Areas of potential difficulty are listed below:

1. Too much flux penetration through the sleeve into the sample region can lead to a number of difficulties. Some flux leakage measurements will be made shortly.

2. Edge effects around the sample could be a serious problem. We have considered a number of plug materials that should confine samples fairly effectively, but they must be tested.

3. There will probably be some difficulties in getting the sleeve and samples cooled, and in the case of hydrogen, obtaining a uniform sample.

4. GMX-1 has offered to help us develop flash x-radiographic techniques to determine the sample volume. Tests should begin

with their equipment shortly. The usefulness of this technique depends strongly upon the resolution that can be obtained.

It is planned to try the first complete experiments with the simple 1.1 MG (50 kb) system. If this system proves usable we would plan to go to the two-stage, 2 MG system which should permit studies to be made at more interesting pressures. Use of the still higher field systems will depend, in turn, upon the success achieved with the 2 MG system.

There are some experiments that can be done which should serve as calibration checks of the diagnostic methods to be used. Many materials, CdS and MnF_2, for example, have pressure transitions well below 50 kb. Large shifts in the absorption edges are expected at the transitions. Of equal interest are the large volume changes ($\geq$ 15%) that can occur there. Spectroscopic techniques already developed can be used to follow the position of the absorption edges as a function of drive field, while abrupt changes in sample volume should be observable from flux pickup loops which surround the sample. These materials are eminently suitable for studying our 1.1 MG (50 kb) simple strip system. Silver chloride, with a transition at 100 kb, should be suitable for making similar studies with the 2 MG system. Other materials are no doubt available for studying the higher field systems.

The accuracy with which the measurements can be made is not known definitely at this time, but some estimates can be made. Drive pressures can be determined to within an error of $\pm$ 3%. Barring significant flux leakage the sample pressures should be calculable to nearly the same accuracy, say $\pm$ 4%. The accuracy with which the volume can be measured is less certain. GMX-1 people feel that the radius can be determined to within $\pm$ 0.2 mm (possibly to within $\pm$ 0.1 mm). For relatively incompressible samples, with initial diameters of about a centimeter, the sample area could then be determined to within 3-5%. For highly

compressible materials the error limits are correspondingly greater. However, the differences between shock and isentropic compression are also greater, as is the isentropic compression predicted by different models, in the case of hydrogen. Here it appears that an uncertainty in volume as large as 15% would still be helpful in discriminating between various models.

FIG 3

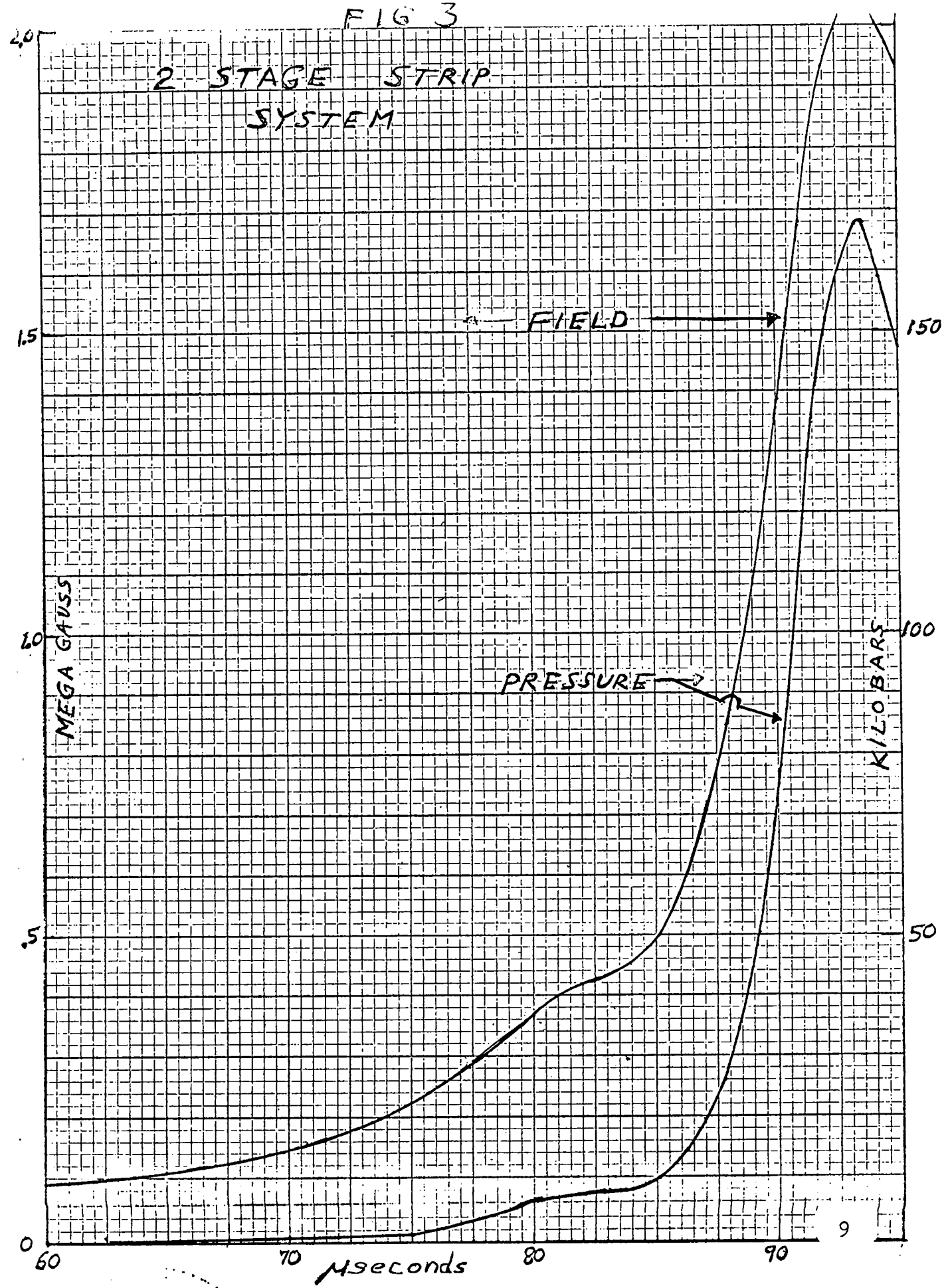
2 STAGE STRIP SYSTEM
FIELD
PRESSURE
MEGA GAUSS
KILO BARS
2.0
1.5
1.0
.5
0
150
100
50
60
70
80
90
Mseconds

Excerpted from

Los Alamos Scientific Laboratory

Internal Document GMX-6-786,

May 1971

Magnetically Driven Compression Studies - W.B.Garn, R.S.Caird, C. M. Fowler

Eight shots have been fired in the program to develop a magnetically-driven system for measuring isentropic equations of state. The work to date has been directed towards finding a suitable liner (driver) material capable of being compressed magnetically by our strip generators while excluding flux from the experimental volume. Also, GMX-1 has been cooperating with us to perfect the x-ray technique necessary to record the inside diameter of the collapsed liners under dynamic conditions. This will define the outside diameter of the less dense compressed samples.

Laboratory experiments indicated that high purity aluminum cooled to about 6.5 $^{\circ}$K temperature becomes an extremely good conductor and should make an excellent driver material. Four 2 MG high field explosive shots using a cold (6.5 $^{\circ}$K) high purity 1 mm wall aluminum liner have verified the laboratory data by showing very little leakage field. X-ray pictures were taken during two shots; for one the Al liner was filled with paraffin and for the other foam plastic. Both x-ray films were recovered but no usable information was obtained. The compressed paraffin was apparently too dense for the available x-ray energy and the other film (a more sensitive type) was blackened either by shock or improper handling.

The cryogenics group (P-8) has cooperated with us by designing a liner-container cell to permit magnetic compression of liquid hydrogen using our high field strip systems. Aluminum has difficult fabrication problems so we have decided to try using Cu liners. Four shots have been fired, three with 1 mm wall Cu liners, and one with a 1/2 mm wall liner. A sketch of the experimental system is reproduced as Figure 1. For leakage field

measuring shots, three magnetic probes are used to simultaneously measure the drive field, leakage field and the liner diameter. When an x-ray picture of the collapsed liner is taken, the leakage probe is omitted. Figure 2 shows typical integrated voltage records obtained from these three probes. The drive field follows the typical strip generator output curve starting with a low initial value of about 70 kG and increasing to 1.1 to 2 MG depending upon the system used. For cold copper (6.5 $^{\circ}$K) the leakage field starts and remains less than 3% of the drive field until the liner begins to collapse. This collapse rapidly compresses the leakage flux to a value about 8% of the drive field at leakage probe destruction time. This leakage is within usable limits. The third probe or flux loop is initially wound tightly around the liner so that its effective area starts very small and increases as the liner collapses. By knowing the value of the drive field and the flux loop voltage at any particular time, the area between the flux loop and the liner outer surface can be calculated. This gives a measure of the outer liner diameter. The flux loop voltage (Fig. 2) increases smoothly from a very small value (minimum area between the loop and the liner) to an inflection at a time which corresponds closely with complete liner collapse. A slight decrease in voltage occurs at this time indicating a possible expansion of the liner. An x-ray picture was taken during one (1 mm wall Cu) shot and was successful. Figure 3 is a reproduction of the x-ray of the setup (uncollapsed liner) and the shot (partially collapsed liner). The diameter of the central dark spot represents the inner surface of the Cu liner. An area decrease of about 6 to 1 is represented by these pictures. X-ray timing was intentionally set before complete collapse time in order to observe the inner surface symmetry. The uniformity and symmetry of the collapse appears to be excellent. Concentric circles result from the insulation spaces between the high field coil, glassware and liner. These rings do show that the liner remains well centered during the collapse.

The first two assemblies suitable for use for compression of liquid hydrogen have been delivered from the fabrication group (CMB-6). These cells use 1 mm wall Cu as the liner-driver with beryllium end caps for minimum x-ray attenuation. A sketch of these cells is reproduced as Figure 4.

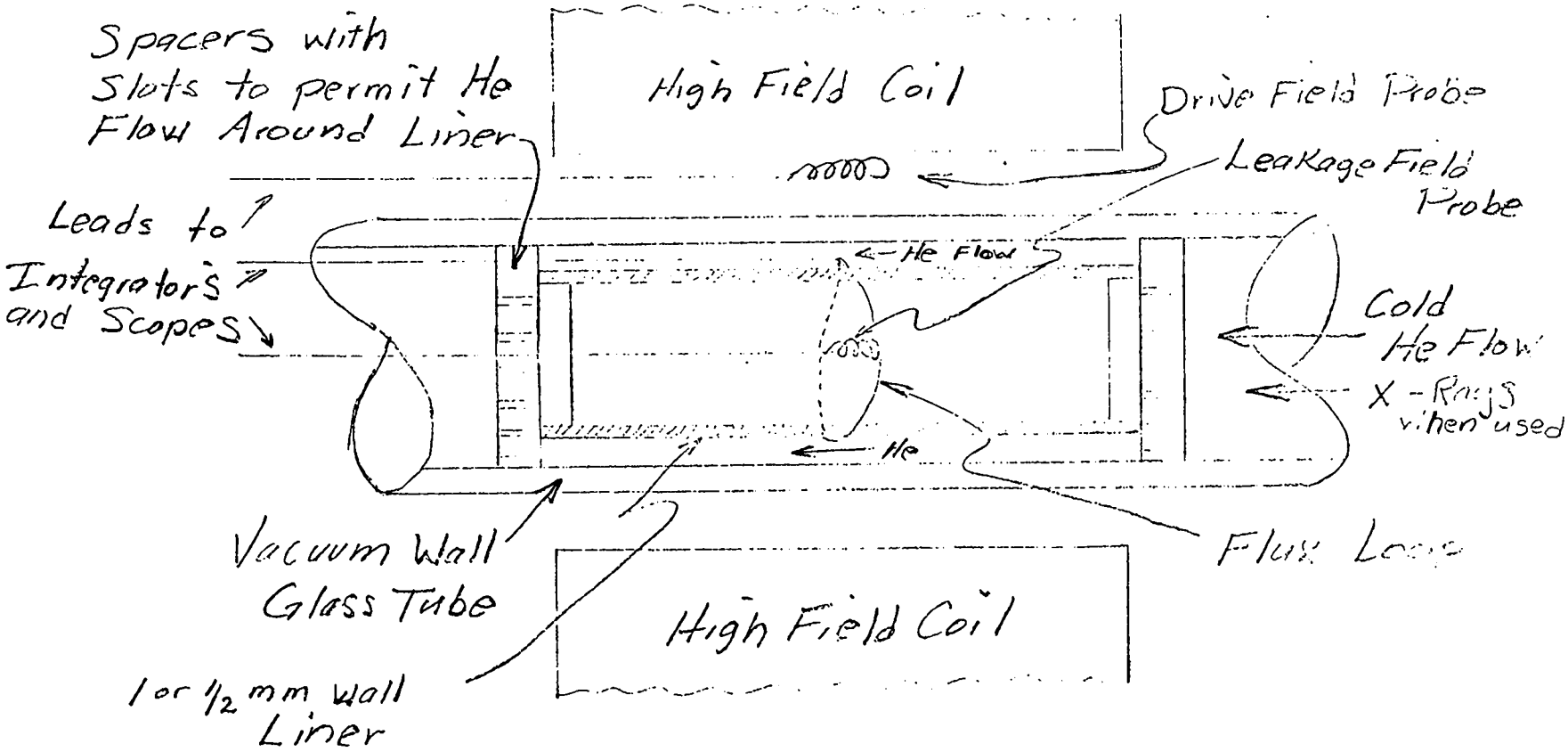

Liner and Probes

Figure 1

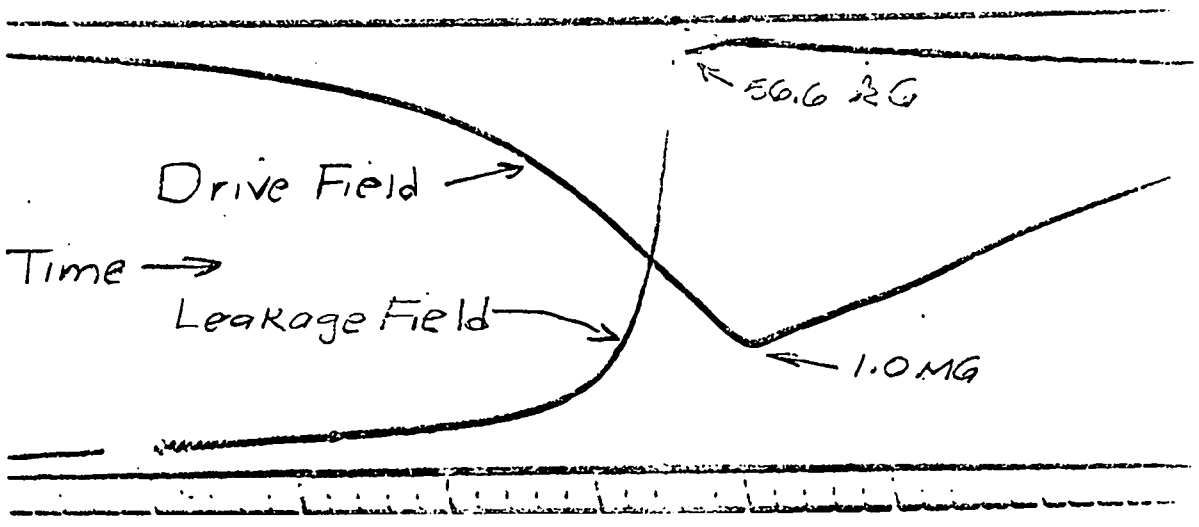

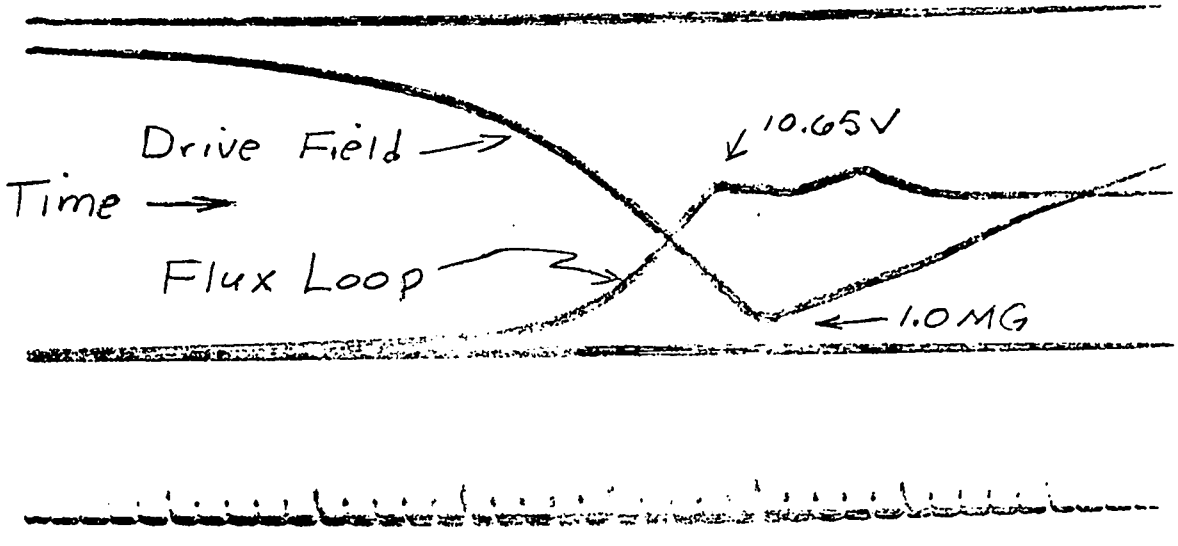

Typical Records
Figure 2

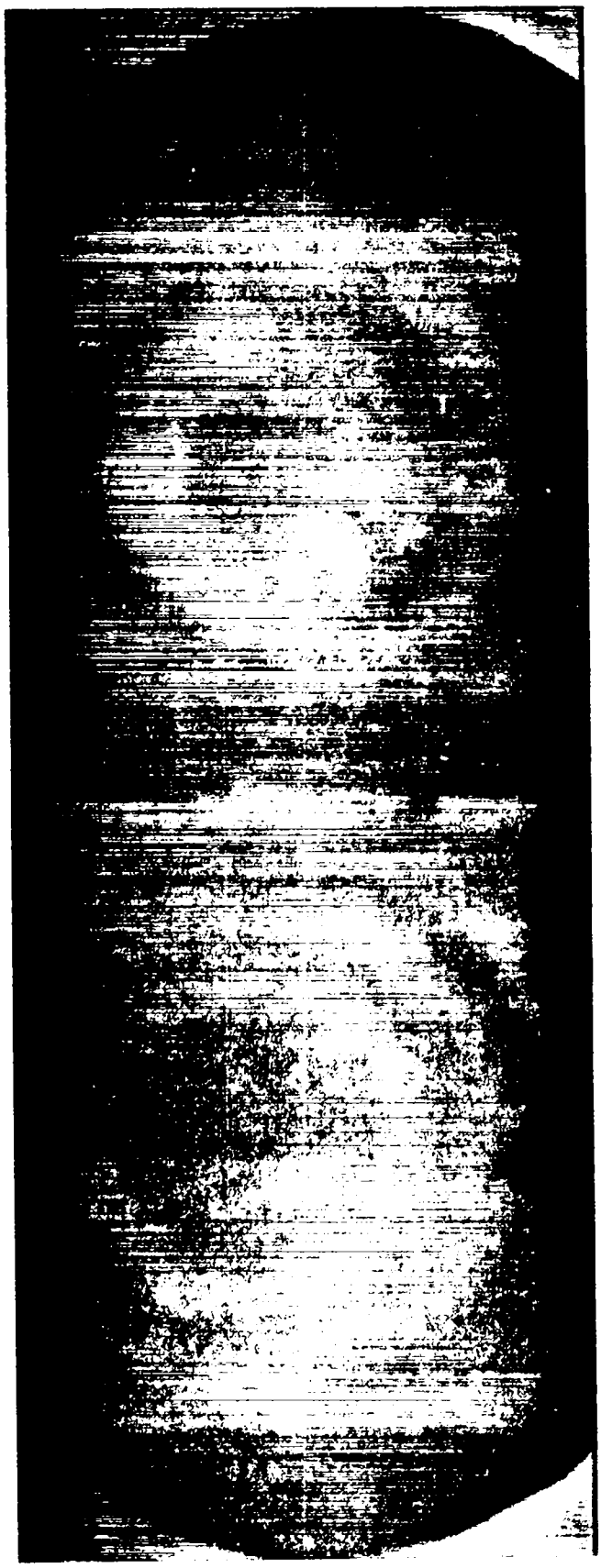

Figure 3

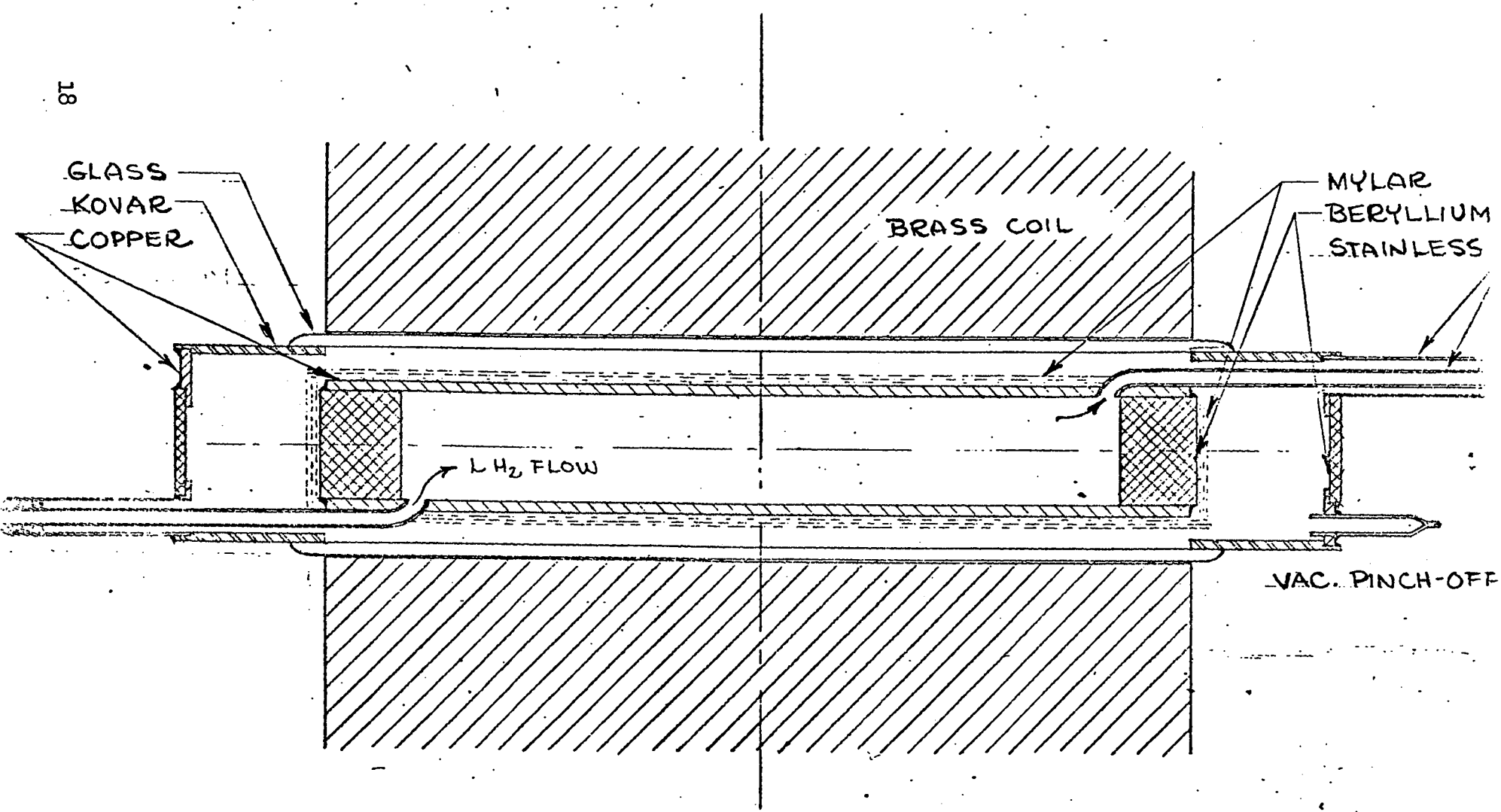

MAGNETIC IMPLOSION CELL

SCALE = 2 X SIZE

Figure 4

Excerpted from

Los Alamos Scientific Laboratory

Internal Document GMX-6-384,

April 1958

2. VOLTAGE GENERATION OF IMPLODING MAGNETIC FIELDS - C. M. Fowler, W. B. Garn.

A. Summary and Introduction.

Some interest has arisen recently concerning the use of imploding magnetic fields to generate high voltages, and to accelerate charged particles. These and some other questions have been investigated in this report.

In Section C calculations are given for the induction of voltages in pickup coils contained in imploding magnetic fields. With cylindrical implosions it appears possible to generate voltages in the hundred kilovolt range, using pulsed initial magnetic fields. A few kilovolts should be fairly easily obtained with a plane implosion employing permanent magnets to produce the initial field.

Section D treats some examples of ion accelerations in imploding fields. It is found that the ions are accelerated in such a fashion that initial energies are multiplied by the field compression. For cylindrical implosions, multiplications of a few hundred seem possible. Multiplications of only 10 to 50 appear possible for plane implosions, but the ion injection problem is simplified.

Section B discusses, in some detail, the validity of the "flux conservation approximation" which is employed in Sections C and D.

B. The Flux Conservation Approximation.

The build up of magnetic and electric fields in vacuum, that result from the implosion of magnetic fields trapped by perfect conductors, occurs by the propagation of electromagnetic waves between the field boundaries. Examples of such fields are given in GMX-6-381. Although the analyses presented in that report are precise, within the rather rigorous limitations imposed upon the solutions, the results are usually complicated. The work required to extend these results to more complicated situations, such as the calculation of ion orbits in the fields, is almost prohibitive.

There exists, however, an approximate method of treating these problems, based upon the conservation of magnetic flux within the perfect conductors. As an aid in studying this approximation, the results of Example 2 of GMX-6-381, page 16 are summarized below. Figure 2 of that report is also reproduced and relabeled Fig. 1 of the present report.

This figure presents in characteristic form, the E and B fields induced by the plane implosion of two perfectly conducting plates, enclosing an initially uniform field, B_o. For convenience, the initial field is given the value $B_o = 1$. The planes are separated initially by 1 unit, and are imploded towards each other with a velocity $v = .02$. Velocity units are normalized to light velocity $c = 1.000$. The abnormally high implosion velocity was employed to show changes of fields in a reasonable number of electromagnetic wave cycles between the conducting walls.

Inspection of Fig. 1 shows that the fields have constant values within x-t zones, the magnetic fields being symmetric about the center, the electric fields antisymmetric.

Previous Eqns. (c.7), (c.8) and (c.10) give values of the magnetic field in the i^{th} central zone, the time starting the i^{th} central zone, and the value $(\frac{\Delta B}{\Delta t})_i$ for central zones respectively. These equations are reproduced as (B.1-3) below

$$B_i = \left(\frac{1+\nu}{1-\nu}\right)^i B_0 \tag{B.1}$$

$$t_i = \frac{1}{2\nu} - \frac{1+\nu}{2\nu}\left(\frac{1-\nu}{1+\nu}\right)^i \tag{B.2}$$

$$\left(\frac{\Delta B}{\Delta t}\right)_i = \frac{2\nu}{1-\nu}\left(\frac{1+\nu}{1-\nu}\right)^{2i} B_0 \tag{B.3}$$

To these equations may be added the value of E_i for the left lateral zones

$$E_i = \frac{\nu B_0}{(1-\nu)^{2i}} \tag{B.4}$$

Referring now to Fig. 1, consider a rectangular pickup coil, of length b in the y direction, but of width 2x in the x direction and centered about x = .5. The electromotive force around the coil is zero for times when the coil is in the central x-t zones. When the coil is in the lateral x-t zones, the electromotive force has the value

$$\mathcal{E}_i = -2bE_i = \frac{-2b\nu B_0}{(1-\nu)^{2i}} \tag{B.5}$$

This result follows from subtraction of $+bE_i$, the electromotive force around the right-hand boundary from $-bE_i$, the value along the left-hand boundary.

Of more interest is the time average emf around the coil between zones. Reference to Fig. 1 shows that between times t_{i+1} and t_i, the emf is zero except for the time Δt, given below, when it has the value given by (B.5)

$$\Delta t = \frac{2\gamma}{C} = 2\gamma \quad ; \quad (C = 1) \tag{B.6}$$

The average emf is then given by

$$\hat{\mathcal{E}}_i = -2\ell E_i \left(\frac{\Delta t}{t_{i+1} - t_i}\right) = -2\ell \frac{\nu B_0}{(1-\nu)^{2i}} \frac{2\gamma}{\left(\frac{1-\nu}{1+\nu}\right)^i}$$

Or

$$\hat{\mathcal{E}}_i = -4\ell\gamma \frac{\nu B_0}{(1-\nu^2)^i}\left(\frac{1+\nu}{1-\nu}\right)^{2i} = -2\nu B_0 \frac{(\text{coil Area})}{(1-\nu^2)^i}\left(\frac{1+\nu}{1-\nu}\right)^{2i} \tag{B.7}$$

So far these have been precise results. The approximation method employs the conservation of flux principle. In this example, the flux per unit of y distance is $B_o \cdot 1$. At a later time, the conductors are separated by a distance 1 - 2vt. Thus

$$B(t) \doteq \frac{B_0}{1-2\nu t} \quad ; \quad \dot{B} \doteq \frac{2\nu B_0}{(1-2\nu t)^2} \tag{B.8}$$

Application of Maxwell's equation $\nabla \times \vec{B} = -\frac{\partial \vec{B}}{\partial t}$, with the assumption that $\vec{E} = E\vec{j}$, gives

$$\mathcal{E} = -\gamma \dot{B} \tag{B.9}$$

and

$$\mathcal{E} = -\dot{B}(\text{coil Area}) \tag{B.10}$$

For comparison of the approximate expression (B.8) and B.10) with the precise expressions, we evaluate them at times $t = t_i$. These yield the following

$$B(t_i) \doteq \frac{B_0}{1+v}\left(\frac{1+v}{1-v}\right)^i \tag{B.11}$$

$$\left(\frac{dB}{dt}\right)_{t_i} \doteq \frac{2vB_0}{(1+v)^2}\left(\frac{1+v}{1-v}\right)^{2i} \tag{B.12}$$

$$\mathcal{E}_i \doteq -(\text{Coil Area})\,\frac{2vB_0}{(1+v)^2}\left(\frac{1+v}{1-v}\right)^{2i} \tag{B.13}$$

These expressions are to be compared with (B.1), (B.3) and (B.7). Since v in practice is of the order of 10^{-5}, the approximations all appear good. The expression ftr E of Eqn. (B.9) may be shown to be essentially the time average of the correct E.

Finally, a problem of interest in the experimental work in progress in this field, is the response of a circuit actuated by a pickup coil in the imploded fields. Here the emf's induced in the coil will be considered as arising from the flux change through the coil. For simplicity, the circuit is assumed to be free of resistance. The sketches below illustrate the problem.

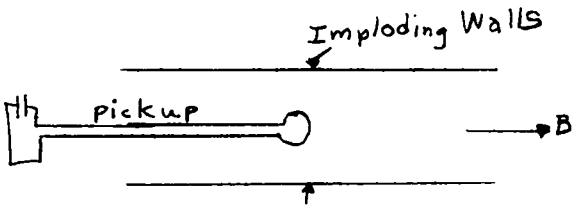

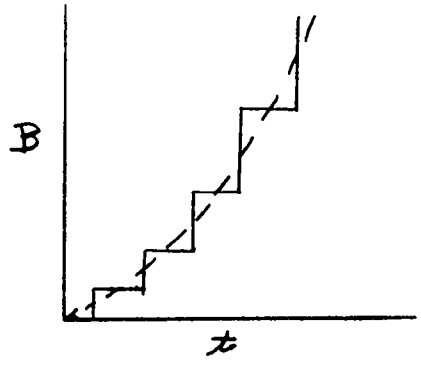

The problem to be considered is this: How nearly does the pickup coil respond to the change of the average B field (shown dotted) when the field actually increases stepwise, as shown in the diagram? The intuitive answer, that the responses are essentially identical if the time constant of the circuit embraces many B steps, will be shown to be correct.

Let A be the coil area, L and C the circuit inductance and capacitance. The differential equation for the charge q in the circuit is:

$$\ddot{q} + \frac{q}{LC} = \frac{A}{L}\frac{\widehat{dB}}{dt} \tag{B.14}$$

Application of the Laplace transform, with $\Phi = \int_0^\infty e^{-zt} q(t)\, dt$, and with the circuit initially uncharged and quiescent, yields

$$\Phi = \frac{A/L}{z^2 + \frac{1}{LC}} \int_0^\infty e^{-zt} \frac{\widehat{dB}}{dt}\, dt \tag{B.15}$$

The current q(t) is given by the usual Bromwich contour integral

$$q(t) = \frac{1}{2\pi i} \int_{Br} e^{zt} \Phi(z)\, dz$$

When the field B occurs in steps B_i at time locations τ_i, as shown in the sketch, (B.15) reduces to

$$\Phi = \frac{A/L}{z^2 + \frac{1}{LC}} \sum_i (B_{i+1} - B_i) e^{-z\tau_i} \tag{B.16}$$

The singularities of Q are simple poles at $Z = \pm i\omega$ ($\omega^2 = \frac{1}{LC}$) and the inversion of (B.16) yields

$$q = \frac{A}{\omega L} \sum_{i=1}^{n} \left(\frac{B_{i+1} - B_i}{\Delta\tau_i}\right) \sin \omega(t - \tau_i)\, \Delta\tau_i$$

$$\tau_n < t < \tau_{n+1} \; ; \; \Delta\tau_i = \tau_{i+1} - \tau_i \tag{B.17}$$

When B varies continusouly, it is easily shown that

$$q = \frac{A}{\omega L} \int_0^t \frac{dB(\tau)}{d\tau} \sin \omega (t-\tau)\, d\tau \qquad \text{(B.18)}$$

Expressions (B.17) and (B.18) become essentially identical under these conditions:

(i) $\frac{dB}{d\tau} \doteq \frac{(B_{i+1} - B_i)}{\Delta\tau_i}$

(ii) $\omega\tau_i$ can be treated as a continuous variable, or $\omega\Delta\tau << 1$

The first condition has been shown to be quite well satisfied. The second condition demands that the circuit time constant include many B steps.

In summary, it appears as though the approximate treatment is adequate in so far as time average values are concerned, and if the inertia of the interacting systems is sufficiently large. It should be remarked that use of $\nabla \times \vec{E} = -\frac{\partial \vec{B}}{\partial t}$ to calculate E fields is inconsistent when $\vec{B}$ is taken as independent of spacial coordinates. The companion Maxwell equation, $\nabla \times \vec{B} = \frac{1}{c^2}\frac{\partial \vec{E}}{\partial t}$ demands a spacial varying B field. However, it can be seen that the magnitude of the spacial B fields required are of the order $\frac{v^2}{c^2}$ B(t), and for the velocities v considered here, may safely be neglected.

C. Production of High Voltages.

The experiments under preparation to produce high voltage incorporate a multiturn pickup coil placed in an imploding cylindrical system with an axial field, as sketched below (Pg. 77).

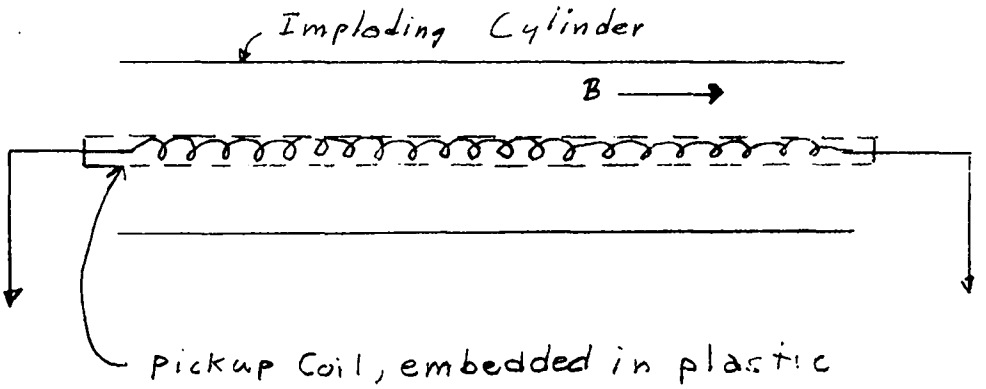

Using the flux conservation equation described in Section B, the emf induced across the coil is given by

$$|\mathcal{E}mf| \doteq n A \frac{dB}{dt} = n A 2\pi R_0^2 B_0 / r^3 \qquad (C.1)$$

Here conservation of the axial flux gives

$$B(t) = B_0 \left(\frac{R_0}{r}\right)^2 = B_0 \left(\frac{R_0}{R_0 - vt}\right)^2$$

Typical values of these quantities are:

n = 50 turns

coil radius = (.5 cm); $A = \pi (5\ 10^{-3})^2 m^2$

$B_0 = 5\ w/m^2$

$R_0 = 2.5\ cm = 2.5\ 10^{-2} m$

$r = .6\ cm = 6\ 10^{-3} m$

$v = 2 \times 10^3 m/sec$

Thus

$$Emf = \frac{(50)(\pi\ 2510^{-6})\ 2(2\times10^3)(2.5\ 10^{-2})^2(5)}{(6\cdot10^{-3})^3} = 227{,}000\ volts$$

These quantities are typical of those that may be expected in the present

experimental facility. The voltage pulse varies inversely with the cube of the implosion radius. However, such factors as flux leakage, two dimensionalty of the field and magnetic pressure deceleration of the walls have not been considered. Further there may be some practical limitations on voltage breakdown between coil turns, which may reduce the number of turns. On the other hand, it may be possible to produce higher peak voltages by using smaller radius coils, and thus allowing a further compression of the field before coil destruction occurs.

Considering now the implosion of plane conductors, it appears, in principle, fairly easy to produce a few thousand volts in a fairly small system, employing a permanent magnet to produce the initial field.

As an example, a theoretical value of 5000 volts may be obtained from a 25 turn pickup coil of .1 x 1 cm cross-section with Comp. B implosion of two conductors 1 cm apart with an initial field of 5000 gauss.

D. The acceleration of Charged Particles in Imploding Fields.

Ion orbits in several kinds of imploding fields are considered in this section. Several approximations are made.

1. Electric and magnetic fields are calculated with the flux conservation approximation outlined in Section B.

2. Single ions are considered. Thus no interaction of particles is taken into account, as would be necessary for heavy ion currents. Similarly, the energy removed from the field by the ion is neglected. For heavy currents, this factor is a limitation on the accelerations possible.

3. Non-relativistic mechanics are employed.

4. Radiation losses are not considered.

The limitations implied by 2.) are clear. For ions, 3.) and 4.) are not serious, since it does not appear possible to accelerate ions to energy

ranges where these factors are significant. Electrons are not considered, but it is almost certain that relativistic mechanics should be used. Further, the orbit curvatures would probably be large. Consequently, radiation losses would have to be investigated.

The validity of the approximation formulas is at present unknown. Analytic solutions both relativistic and non-relativistic are available for the plane implosion case. These are possible because the various x-t zones are regions of constant E and B fields. However, the effort expended in continually reworking the problem for each new zone, with matching at the zone boundaries seems prohibitive at present. This effort is complicated further by the difficulty of finding the zone intersection points. Even in the non-relativistic case, the cycloidal trajectories require solutions of transcendental equations to locate these points. It seems to the writers, intuitively, that the time averaged fields of the approximation method should give an overall picture of the ion orbits. However, the very small masses of the particles allow them to respond even to very rapid field changes. There is then the danger that the equations employed are not sufficiently detailed.

Example 1 Particle in axial cylindrical implosions.

With a field $B = B(t)\vec{k}$ the Maxwell induction equation implies a tangential electric field $E_\theta = -\dot{B}\frac{r}{2}$. The Cartesian components are then given by

$$E_x = \dot{B}y/2 \; ; \quad E_y = -\dot{B}\frac{x}{2} \tag{D.1}$$

The non-relativistic Lorentz force equation, $m\ddot{\vec{r}} = q(\vec{E} + \vec{v} \times \vec{B})$ gives as the equations of motion for an ion of mass m, charge q:

$$m\ddot{x} = q(\dot{B}y/2 + B\dot{y}) \tag{D.2}$$

$$m\ddot{y} = -q(\dot{B}x/2 + B\dot{x}) \tag{D.3}$$

$$m\ddot{z} = 0 \tag{D.4}$$

For a uniform implosion velocity v, initial field B_o and initial radius r_o, the field B is given by

$$B(t) = \frac{B_o}{(1 - \frac{v}{r_o} t)^2} \tag{D.5}$$

The ion velocity in the axial directions is constant. The general solutions of (D.2) and (D.3) are found to be

$$x = \tau \left[a_o + c_o \cos \frac{\mu}{\tau} + c_1 \sin \frac{\mu}{\tau} \right] \tag{D.6}$$

$$y = \tau \left[a_1 + c_1 \cos \frac{\mu}{\tau} - c_o \sin \frac{\mu}{\tau} \right] \tag{D.7}$$

with $\mu = q B_o r_o / m v$

$$\tau = 1 - \frac{v}{r_o} t \tag{D.8}$$

Without loss of generality, we may take $y_o = 0$, $\dot{x}_o = 0$, $x(0) = x_o$, $\dot{y}(0) = v_{oy}$. The solutions for x and y become

$$x = \tau \left[x_o + \frac{x_o}{\mu} \sin \left(\frac{\mu}{\tau} - \mu \right) + \frac{r_o v_{oy}}{\mu v} \left\{ 1 - \cos \left(\frac{\mu}{\tau} - \mu \right) \right\} \right] \tag{D.9}$$

$$y = \tau \left[\frac{x_o}{\mu} \left\{ \cos \left(\frac{\mu}{\tau} - \mu \right) - 1 \right\} + \frac{r_o v_{oy}}{\mu v} \sin \left(\frac{\mu}{\tau} - \mu \right) \right] \tag{D.10}$$

Figure 2 shows the orbit of a deuteron calculated with the following specific values: $x_o = 4$ cm, $r_o = 5$ cm, $v_{oy} = 10^7 \frac{\text{cm}}{\text{sec}}$, $B_o = 510$ gauss, v implosion = 5 mm/μsec. The initial field value was chosen to orbit the deuterons at a 4 cm radius initially. At smaller values of τ, it may be shown that the initial energy is multiplied by the factor $\frac{1}{\tau^2}$, assuming that

the initial ion injection was essentially transverse to the field. This is necessary, at any rate, in order to keep the axial translation during the collapse time small enough for a practical system.

Example 2 Ions in plane imploding field

From a practical viewpoint transverse ion injection between two planes appears easier than injection into a cylindrical cavity. Although energy multiplication is less efficient for the plane implosion, this and other factors make this study plausible.

Taking the B field as $B(t)\vec{k}$, the Maxwell induction equation yields $\vec{E} = -x\dot{B}\vec{j}$. The Lorentz force equation gives as the ion equations of motion:

$$\ddot{x} = \frac{q}{m} \dot{y} B \tag{D.11}$$

$$\ddot{y} = -\frac{q}{m} (x\dot{B} + \dot{x}B) \tag{D.12}$$

$$\ddot{z} = 0 \tag{D.13}$$

For the implosion of planes, with relative conductor velocity v, initial separation a, and initial uniform field B_o, the expression for B(t) becomes

$$B(t) = \frac{B_o}{1 - \frac{v}{a}t} \tag{D.14}$$

Details of the solutions of (D.11-13) with the field (D.14) will be omitted. The solutions are most easily expressed in terms of the reduced parameters given below.

Definitions:

$$k = v/a \qquad \alpha = v_{oy} + \omega_o x_o \text{ (constant of integration arising from (D.12))}$$

$$\tau = 1 - (v/a)t = 1 - kt \qquad L = \alpha/k$$

$$\omega_o = \frac{B_o q}{m} \tag{D.15}$$

$$K = \omega_o/k$$

The general solutions become:

$$x = \frac{1}{\kappa}\tau + \sqrt{\tau}\left[A\cos\left(\sqrt{\kappa^2-1/4}\log\tau\right) + D\sin\left(\sqrt{\kappa^2-1/4}\log\tau\right)\right] \qquad (D.16)$$

$$y = \beta + \frac{\sqrt{\tau}}{2\kappa}\left[\left\{\cos\left(\sqrt{\quad}\log\tau\right) + 2\sqrt{\kappa^2-1/4}\sin\left(\sqrt{\quad}\log\tau\right)\right\}A + \left\{\sin\left(\sqrt{\quad}\log\tau\right) - 2\sqrt{\kappa^2-1/4}\cos\left(\sqrt{\quad}\log\tau\right)\right\}D\right] \qquad (D.17)$$

Inspection of (D.16) and (D.17) shows that the ion orbits each time the argument $\sqrt{\kappa^2-1/4}\log\tau$ goes through 2π. When this value is $-n\pi$,

$$\tau = e^{-\frac{n\pi}{\sqrt{\kappa^2-1/4}}} \quad ; \quad t = \frac{1}{\kappa}\left[1 - e^{-\frac{n\pi}{\sqrt{\kappa^2-1/4}}}\right] \qquad (D.18)$$

If we neglect the Z component of kinetic energy, and take the initial transerse velocity as v_{oy}, the kinetic energy for small values of τ given by (D.18) may be shown to be very closely

$$K.E. \doteq \frac{1}{2}m v_{oy}^2 e^{\frac{n\pi}{\sqrt{\kappa^2-1/4}}} \doteq (K.E.)_o e^{\frac{n\pi}{\sqrt{\kappa^2-1/4}}} = \frac{(K.E.)_o}{\tau} \qquad (D.19)$$

It is also assumed here that $K^2 \gg 1$.

As a typical example, consider ionized deterons, initial field 10,000 gauss, relative liner velocity 2 mm/μsec and initial spacing of 5 cm. Then:

$$\omega_0 = \frac{qB}{m} = .479\,10^8\ \text{sec}^{-1}$$

$$\kappa = \frac{v_{liner}}{a} = 4\cdot10^4\ \text{sec}^{-1}$$

$$K = \frac{\omega_0}{\kappa} = 1.20\ 10^3$$

Under the conditions outlined for this example, it can be shown that the x and y ion coordinates never depart appreciably from those of the injection point.

Theoretically, very high plate compressions should be possible. Suppose practical limitations would still allow reasonable focussing at 95% compression (a total leeway of 2.5 mm about the x and y injection axes). At this point in the compression,

$$\tau = 1 - kt = 1 - .95 = .05$$

$$t = .95/k \doteq 26\ \mu\text{sec}$$

$$\frac{1}{\tau} = e^{\frac{n\pi}{\sqrt{k-1/4}}} = 20$$

$$n \doteq 1140, \text{ or } 570 \text{ ion revolutions}$$

There is, then, an energy magnification of 20. It would appear that only under the most favorable conditions could a factor of 50 be realized. The ions must also be injected in such a manner that the axial motion will not outrun the physical Z dimension in the allotted time. (In this case about 26 μsec for an energy magnification of 20.)

As far as energy multiplication is concerned, the initial field value is largely immaterial within large limits. This factor would allow a considerably larger initial system for the same field source, at the expense of weakening the initial field. This in turn would allow greater compression, and thus greater energy multiplication. However, there is the danger here of not confining the earlier orbit stages within the physical system. This point would have to be investigated more closely.

Example 3 Tangential magnetic field implosion

The implosion of tangential magnetic fields (those produced by currents flowing in a coaxial conductor) lead to fairly high axial electric fields. Some solutions have been obtained for ion motion in these fields. Conservation

of angular momentum is a consequence of these equations, and the solutions so far obtained required the angular momentum to be zero. This confined the motion to a plane, containing the cylinder axis.

The energy multiplication factors are disappointingly low, because of the practical limitation on the axial space dimension. Unlike Example 1, where the accelerations were tangential, here they are axial.

Further calculations would best be done by machine, especially to investigate the influence of angular momentum. If the radial motion is convergent, it is possible that appreciably more acceleration is possible with ions possessing angular momentum.

Axial voltages of the order of 10^7 or more volts/meter are theoretically possible. It would appear as though electrons could possibly be accelerated to the Mev range if properly injected.

Fig. 1

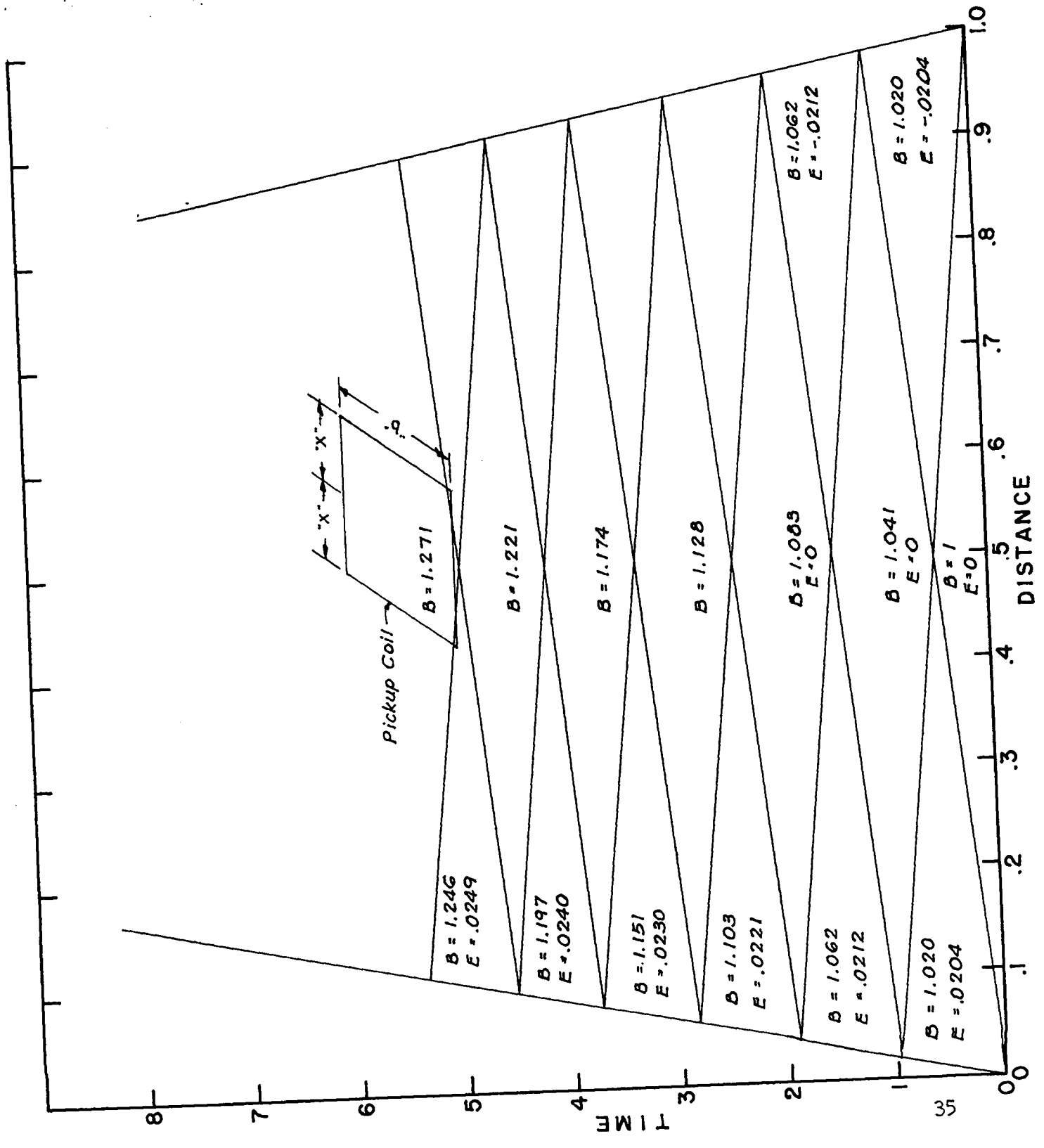
TIME
DISTANCE
Pickup Coil
"x"
"x"
B = 1.271
B = 1.221
B = 1.174
B = 1.128
B = 1.083
E = 0
B = 1.041
E = 0
B = 1
E = 0
B = 1.062
E = -.0212
B = 1.020
E = -.0204
B = 1.246
E = .0249
B = 1.197
E = .0240
B = 1.151
E = .0230
B = 1.103
E = .0221
B = 1.062
E = .0212
B = 1.020
E = .0204

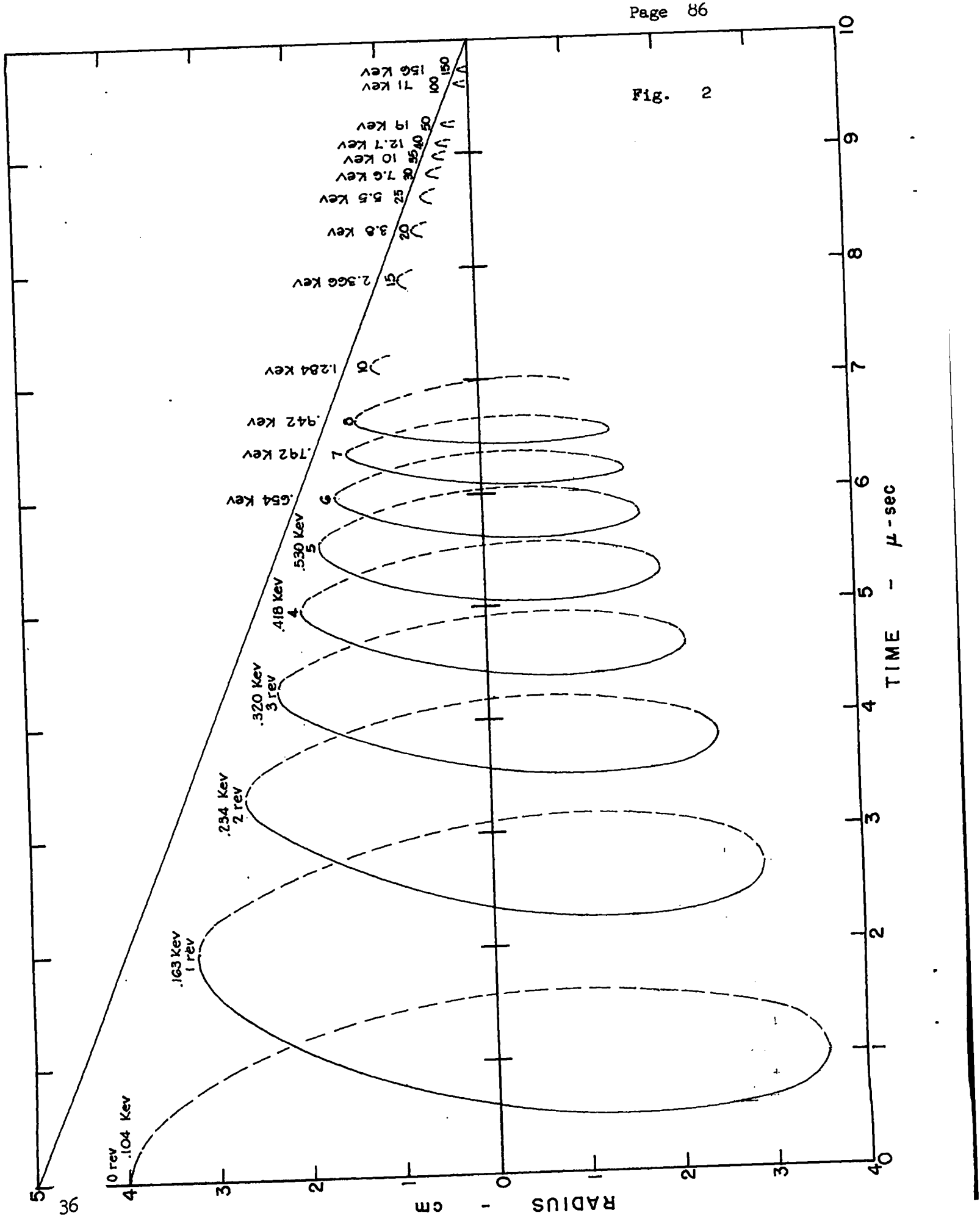
.104 Kev
10 rev
.163 Kev
1 rev
.234 Kev
2 rev
.320 Kev
3 rev
.418 Kev
4
.530 Kev
5
.654 Kev
6
.792 Kev
7
.942 Kev
8
1.284 Kev
10
2.366 Kev
15
3.8 Kev
20
5.5 Kev
25
7.6 Kev
30
10 Kev
35
12.7 Kev
40
19 Kev
50
71 Kev
100
156 Kev
150
RADIUS - cm
TIME - μ-sec

Fig. 2

Excerpted from

Los Alamos Scientific Laboratory

Internal Documents

GMX-6-627, December 1966,

and

GMX-6-662, June 1968

C. Magnetic Program (cont)

Magneto-Resistance of Bismuth- C. M. Fowler, D. B. Thomson, R. S. Caird and W. B. Garn

Work has been started to measure the longitudinal magneto-resistance effect for polycrystalline bismuth in the megagauss magnetic field region, and at a temperature of approximately 300° K.

Preliminary experiments have been performed in the laboratory using the system shown in schematic as Figure 1.

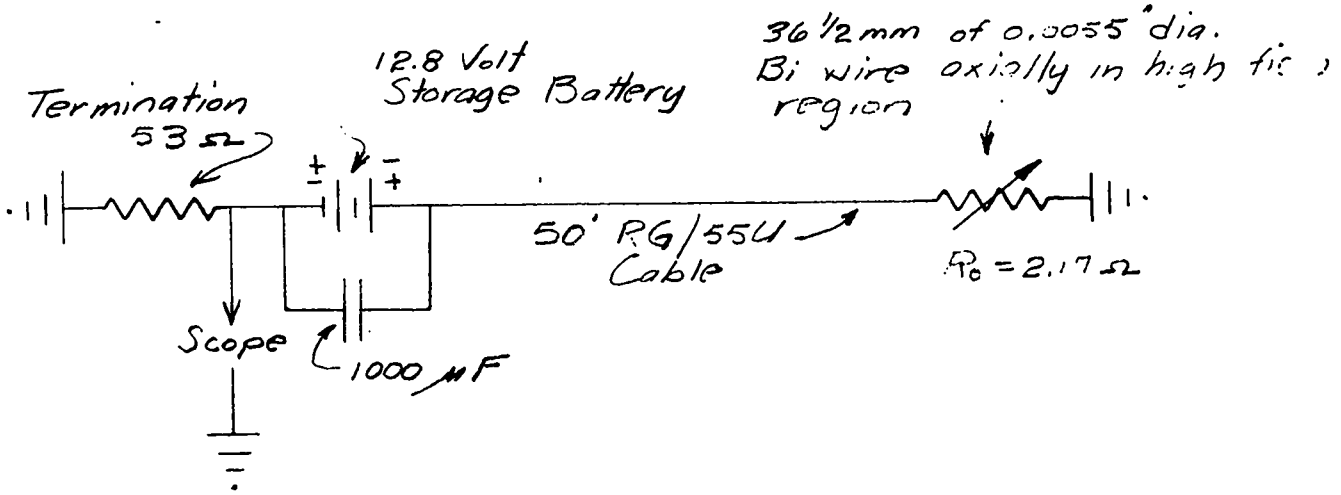

Figure 1.

The Bi wire sample, which is indicated in the schematic as a variable resistance, was inserted axially into a laboratory pulsed-field coil. Peak fields were applied which varied from 15 to 115 kG. EMF pickup from small loops resulting from the necessity of mounting the sample to a signal cable produced sizable noise signals. This pickup unfortunately is comparable in magnitude to the desired signal. Figure 2 is a reproduction of a typical laboratory record. Three bits of information are recorded: The bottom pair of traces was obtained with the battery and capacitor (Fig. 1) removed from the circuit. The upper trace of this pair represents a pure noise signal. The lower trace of each pair gives a B_z probe record for measuring the field. For this record the first peak represents about 95 kG.

With the battery first connected with one polarity and then with reversed polarity (Fig. 1), the two additional magneto-resistance records are obtained (upper traces). By subtracting out the unwanted noise (lower trace) from the magneto-resistance signals at the field peaks, a voltage measurement (e) is obtained which relates to the change in resistance of the sample (R_m) as per Eq. 1.

$$\frac{e}{R_t} = \frac{E}{R_t + R_o} - \frac{E}{R_t + R_o + R_m} \tag{1}$$

e = measured voltage across sample (scope record)

E = known battery voltage, 12.8 volts

R_t = terminator resistance, 53 Ω

R_o = zero field initial resistance of Bi sample, 2.17 Ω

R_m = change in resistance of sample resulting from magneto-resistance effect.

This setup is essentially a constant voltage system with the maximum signal limited to 12.8 volts by the battery. The particular battery value of around 12 volts was chosen to limit the d.c. current through the Bi sample to a safe value of 0.250 amperes.

Records were obtained using bank voltages from 5 to 18 kV which gave field peaks from about 15 kG to 115 kG. These data are plotted in Fig. 3. A considerable amount of scatter is evident in these preliminary data points. However, a definite magneto-resistance effect is observed. At the present time it is not known if the results are consistent with data obtained by earlier investigators. The apparent curvature of this plot may or may not be real. An improved system is being developed which should reduce the data scatter. This arrangement will be discussed in a later paragraph.

Figure 2. A typical record obtained using the circuit shown in Fig. 1. The lower trace of each pair is a B_z probe signal. The upper trace of the lower pair records the pickup with no current flowing in the system. The remaining upper traces are signals obtained with the battery connected first in one direction and then reversed. A voltage signal resulting from the magneto-resistance effect is obtained by subtracting the pickup from the two upper traces. Data were obtained at each of the three field peaks.

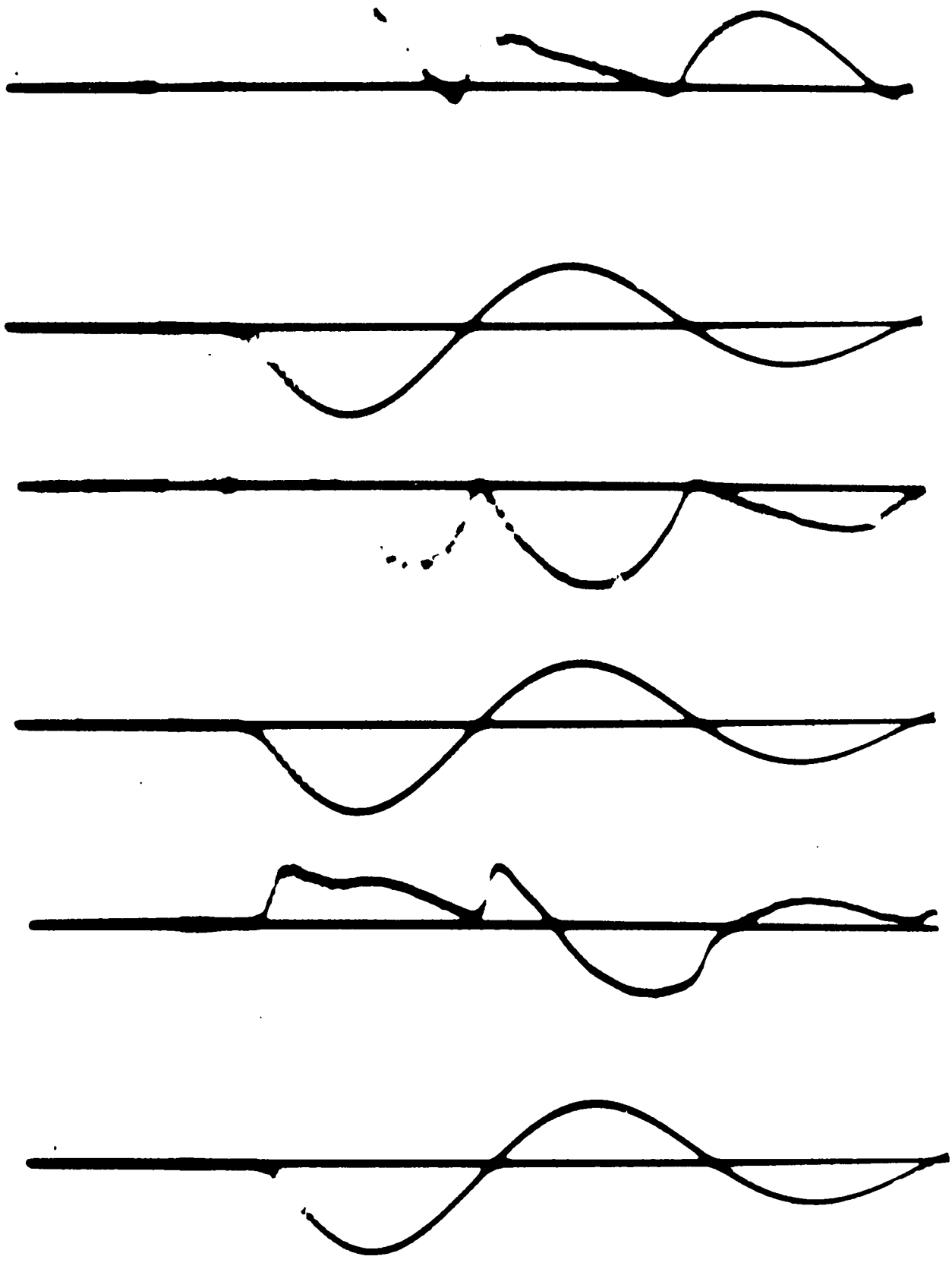

Figure 2.

Figure 3. A plot of preliminary laboratory data showing the longitudinal magneto-resistance effect in polycrystalline bismuth at about 300° K. R/R_o is the ratio of the magnetic contribution to the initial resistance. The test sample consisted of 36 1/2 mm of 0.0055" dia. Bi wire with an initial resistance of 2.17 ohms. The bismuth wire is rated at 99.9% purity.

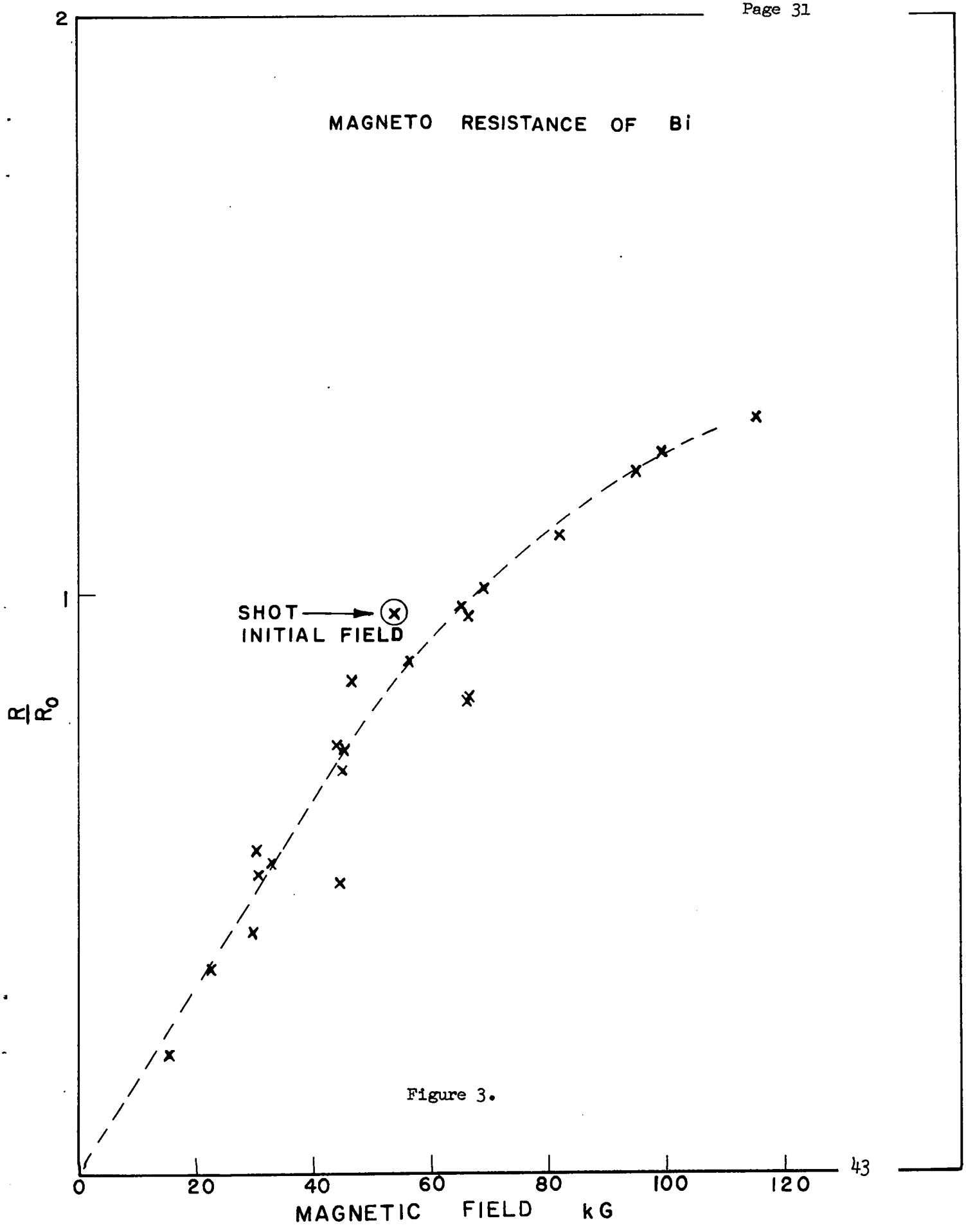
MAGNETO RESISTANCE OF Bi
2
1
R/R0
SHOT
INITIAL FIELD
0
20
40
60
80
100
120
MAGNETIC FIELD kG
43

Figure 3.

On the strength of the laboratory results, an explosive high field experiment was performed. This shot used the identical system from which the laboratory data were obtained (Fig. 1) except the high field coil was replaced by a small strip flux compression system (peak field about 1 MG). The explosive experiment performed operationally correctly and a magneto-resistance measurement was obtained for the initial field conditions. This point is plotted on Fig. 3 and is indicated by a ⊙. The higher field portions of this record have not as yet been satisfactorily analyzed but it is evident that the noise pickup during the final stage of the rapid field increase is very large.

Even before the explosive test had been fired, an improved system was being developed. This circuit is essentially a constant current system and is shown in schematic form in Fig. 4.

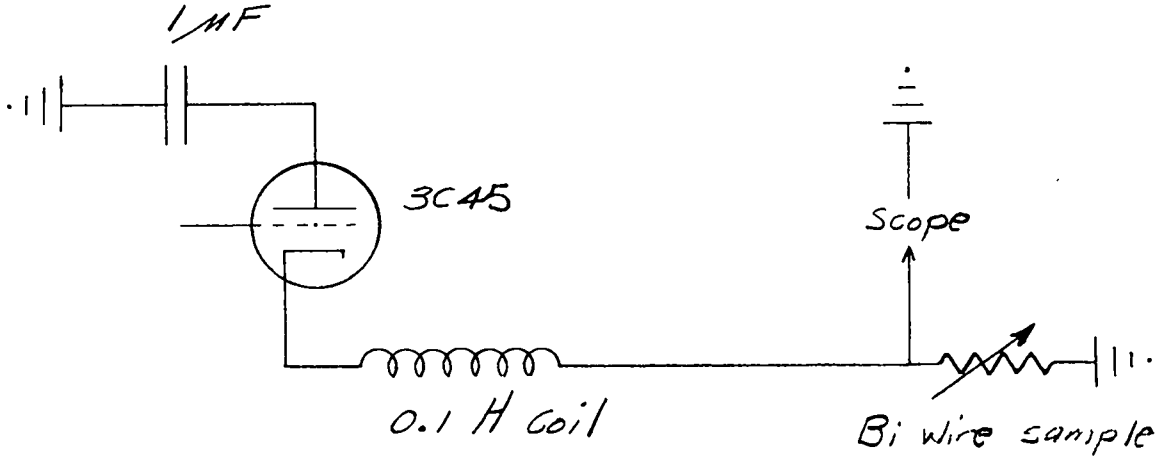

Figure 4.

This arrangement operates in the following manner. The charged 1μF capacitor is dumped through the 0.1 H coil in series with the sample. This current pulse reaches a peak in 500 μsec. Near the current peak where the current flow is quasi d.c. the high magnetic field is applied. The large inductance maintains the current nearly constant while the sample resistance increases, thus producing a voltage signal at the scope proportional to ΔR. This system has

several advantages. It is not limited to a 12 volt maximum signal, and because of the limited energy dumped into the sample, large currents ($\lesssim$6A) can be used repeatedly without damage. This permits a higher signal to noise ratio. A limited amount of laboratory work has indicated this system should perform as expected, and it will be used for the next experimental tests.

Magnetic Program - R. Caird, C. Fowler, W. Garn, D. Thomson

Short reports are given on ~~four~~ two topics. Results from a transverse bismuth magnetoresistance shot are reported in Section 1. It is interesting that the resistivity appears to saturate at about a megagauss at a value 40 times that of the zero field value.

An analysis of a Zeeman doublet obtained up to 1.1 MG for an absorption line in a Nd solution is given in Section 2. Besides the expected linear splitting with the field a quadratic shift of the center of gravity of the lines toward the violet is observed.

1. Transverse Magnetoresistance of Polycrystalline Bismuth at about 20° C

One successful transverse magnetoresistance shot has been fired using an improved sample assembly. A rectangular load coil (1" x 1/4"

cross section) connected to the standard 12" strip flux-compression system provides a convenient experimental volume for this experiment. The peak fields reached are about 1 MG. The technique essentially involves measuring the voltage drop across the Bi sample situated in the increasing transverse magnetic field with a constant current flowing through the sample.

The results of this first shot give data from 55 kG to 1.05 MG for the field increase, and from 1.05 MG down to 0.75 MG for the field decay. The points on the decay curve deviate no more than 2 1/2% from the field rise data. Also, data points were obtained in the laboratory for 20 kG and 55 kG using the same sample. The results of this first shot along with the laboratory data are plotted in Fig. 1. The value of R/R_o plots as a straight line up to about 250 kG, after which deviations begin to appear leading to saturation at about a megagauss. More shots will have to be fired before any attempt will be made to draw conclusions from these data. One possible source of error could be the fine (No. 40) copper lead wires which connect to the sample in the high field region. The initial resistance of these copper leads is comparable with the initial resistance of the Bi sample; however, available handbook data for Cu do not predict much change with field. A future shot will be fired to evaluate the effect of these leads.

2. Zeeman Absorption Spectra of Rare Earth Ions

Neodymium chloride solutions show a sharp but relatively weak absorption line at 4264 Å. A recent high field shot using a concentrated solution gave a very clean record of the absorption spectrum. We were able to measure the splitting of this line up to 1.128 MG. From the voluminous literature available on rare earth ions in solids and liquids, the 4264 Å line has been identified as resulting from a transition from the $^4I_{9/2}$ ground state to a $^2P_{1/2}$ excited state. The measured splitting is considerably larger than that predicted from the free-ion g-values. However, this result is hardly surprising in view of influence of the neighboring water molecules on the Nd^{3+} ion.

The 4264 Å line is split into two components by the magnetic field. The positions of the Zeeman lines were measured with a microscope comparator and converted into wavelength vs. field points. A linear least squares fit of the total separation between the lines gives a total splitting of 21.4 $\mathring{A}$/MG with a standard deviation of about 3%. In addition, there is a shift toward the violet in the center of gravity of the two components. A least squares quadratic fit to this shift indicates a displacement of 5.7 $\mathring{A}/(MG)^2$ toward the shorter wavelengths with an uncertainty of about 1 $\mathring{A}/(MG)^2$. It is interesting to note that some of the other absorption bands show an asymmetric splitting, although we have been unable to obtain good measurements as yet.

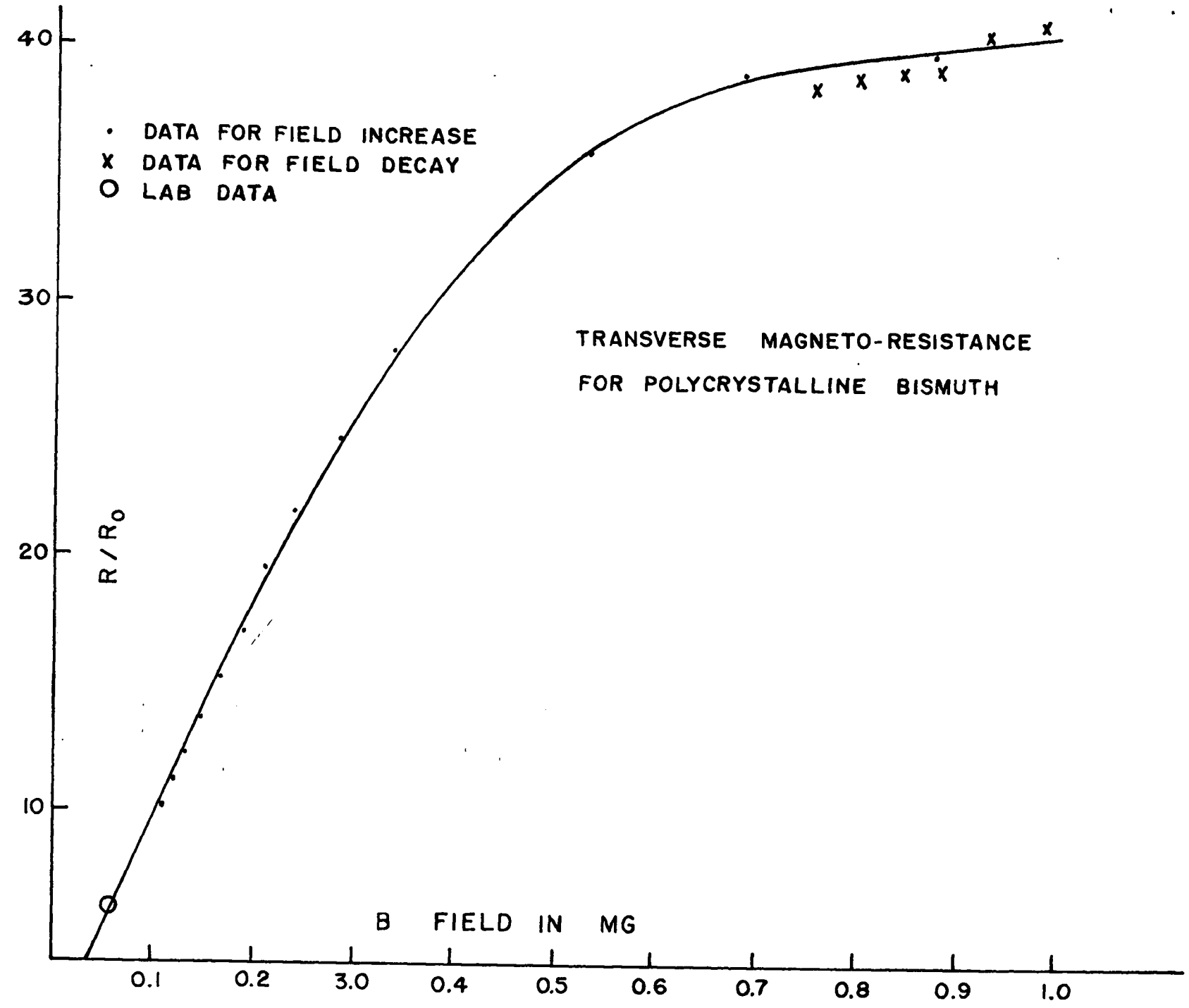
40
30
20
10
R/R₀
• DATA FOR FIELD INCREASE
X DATA FOR FIELD DECAY
O LAB DATA
TRANSVERSE MAGNETO-RESISTANCE
FOR POLYCRYSTALLINE BISMUTH
B FIELD IN MG
0.1
0.2
3.0
0.4
0.5
0.6
0.7
0.8
0.9
1.0

Figure 1.

Excerpted from

Los Alamos Scientific Laboratory

Internal Document GMX-6-718,

August 1969

GMX-6-718
Aug 1967

Absorption Spectrum of GaSe - Magnetic Section

Two records of the time and wavelength resolved transmission spectrum of a GaSe crystal have been obtained. Fig. 1 is the record obtained from a crystal sample estimated to be about 15 microns thick. Wavelengths are determined from the bridge wire spectrum at the right of the photograph, while times and the corresponding magnetic fields are determined from the known spectrographic streak camera writing speed, probe and photomultiplier signals. A complete description of the techniques employed will be given in a later report.

The sample was obtained by cleaving it from a large crystal kindly furnished by John Halpern of the Francis Bitter National Magnet Laboratory. The crystals have a hexagonal structure, and can be cleaved somewhat like mica. The thinnest sections we were able to get were about 10 microns thick, and the second shot was fired with a crystal of this thickness. These shots represent our first exposure to samples that are of uniform thickness (probably to within a small fraction of visible light wave lengths). We were somewhat surprised to see the well formed interference fringes evident on the photograph, which are a consequence of the uniform sample thickness. It is unfortunate that the fringes offer some interference with the main absorption lines, which are of most interest to us. Incidentally, these fringes themselves can be seen to move at large fields when they lie near strong absorption lines, a point of some interest in itself.

Use of the thinner crystal in the second shot did result in moving the fringes further apart (the spacing is roughly proportional to the inverse of the thickness). The quality of the record was rather poor, but we were able to remove some of the ambiguity of the first record. We have talked to various people in CMB-3 about growing thinner crystals for us, using vapor transport methods. W. G. Witteman has made a number of trial batches, continually improving the quality of the crystals obtained. He reports that his latest batch appears quite good. Hopefully, we will have a crystal only a few microns thick for the next shot. Besides

greatly spreading the interference fringes, we anticipate getting better resolved records. It is known that platelets obtained from bigger crystals are strained, whereas the vapor transport grown crystals are essentially strain free, and their absorption spectra have sharper lines.

The magnetic field variation of the absorption peak energies obtained from the two shots may be seen on Fig. 2. The solid line curves up to 175 kG are taken from a paper by K. Aoyagi, et al.[1] We have subtacted 50 wave numbers from their values to bring them into line with our own lower field data. Points labelled by triangles at 100 kG are taken from a paper by Halpern.[2] Two observations may be made about the high field data, both of which need confirmation. First, the change in energy of the level labelled N = 0 is 50 - 75% greater at 1.10 MG than predicted by current theories. Second, it sppears to us that the levels labelled N = 1 and N = 2 are actually doublets, resolved only at the higher fields. If this is true for these levels, it is probable that the higher levels are also doublets, although our resolution is insufficient to prove it. We hope to confirm or refute both of these points with the next experiment. Use of a thinner sample should also allow us to say more about a broader absorption line at 2.14 volts which has been the subject of some discussion.[2] We think this line is visible, but the interference fringes present in both records have, unfortunately, prevented us from obtaining good measurements of its energy variation with field.

Aside from people previously mentioned, we have benefitted from discussions with Dr. J. Halpern of the National Magnet Laboratory, Dr. O. Akimoto of the University of Tokyo, who has supplied us with both reprints and preprints of related work done at that University, and Dr. E. Mooser, now at the Lausanne Federal Polytechnical School, who has also supplied us with a number of reprints and preprints, as well as a prescription for growing GaSe crystals by vapor transport.

[1] K. Aoyagi, et al., Journal of the Physical Society of Japan, Vol. 21, Supplement, p. 174, 1966.

[2] J. Halpern, ibid. p. 180.

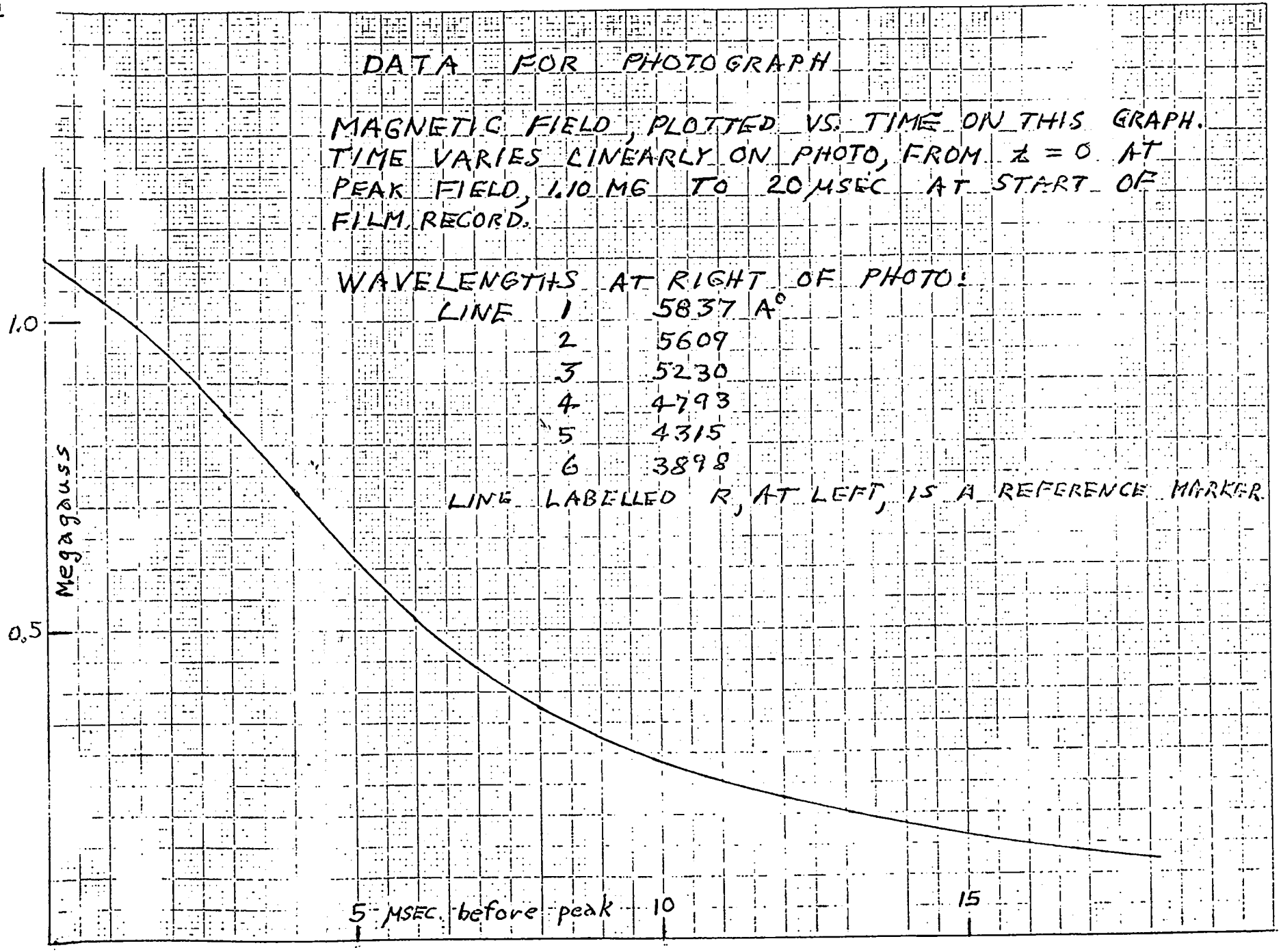
DATA FOR PHOTOGRAPH
MAGNETIC FIELD, PLOTTED VS. TIME ON THIS GRAPH.
TIME VARIES LINEARLY ON PHOTO, FROM t = 0 AT
PEAK FIELD, 1.10 MG TO 20 μSEC AT START OF
FILM RECORD.
WAVELENGTHS AT RIGHT OF PHOTO:
LINE 1 5837 A°
2 5609
3 5230
4 4793
5 4315
6 3898
LINE LABELLED R, AT LEFT, IS A REFERENCE MARKER.
1.0
0.5
Megagauss
5 μSEC. before peak
10
15

Figure 1. Time Resolved, Spectrograph of the Transmission Spectrum of GaSe at 6.5°K.

Wave lengths are obtained from the known bridge wire spectrum shown at the right of the figure, and vary linearly from about 3600A° at the top of the record to 6400A° at the bottom. Time increases linearly from left to right. The time varying magnetic field increases in a non-linear fashion from 110 kG at the left hand side of the figure to 1.10 MG at the peak where the spectral lines are shifted the most. After peak, the field decays gradually to about a megagauss at the end of the record.

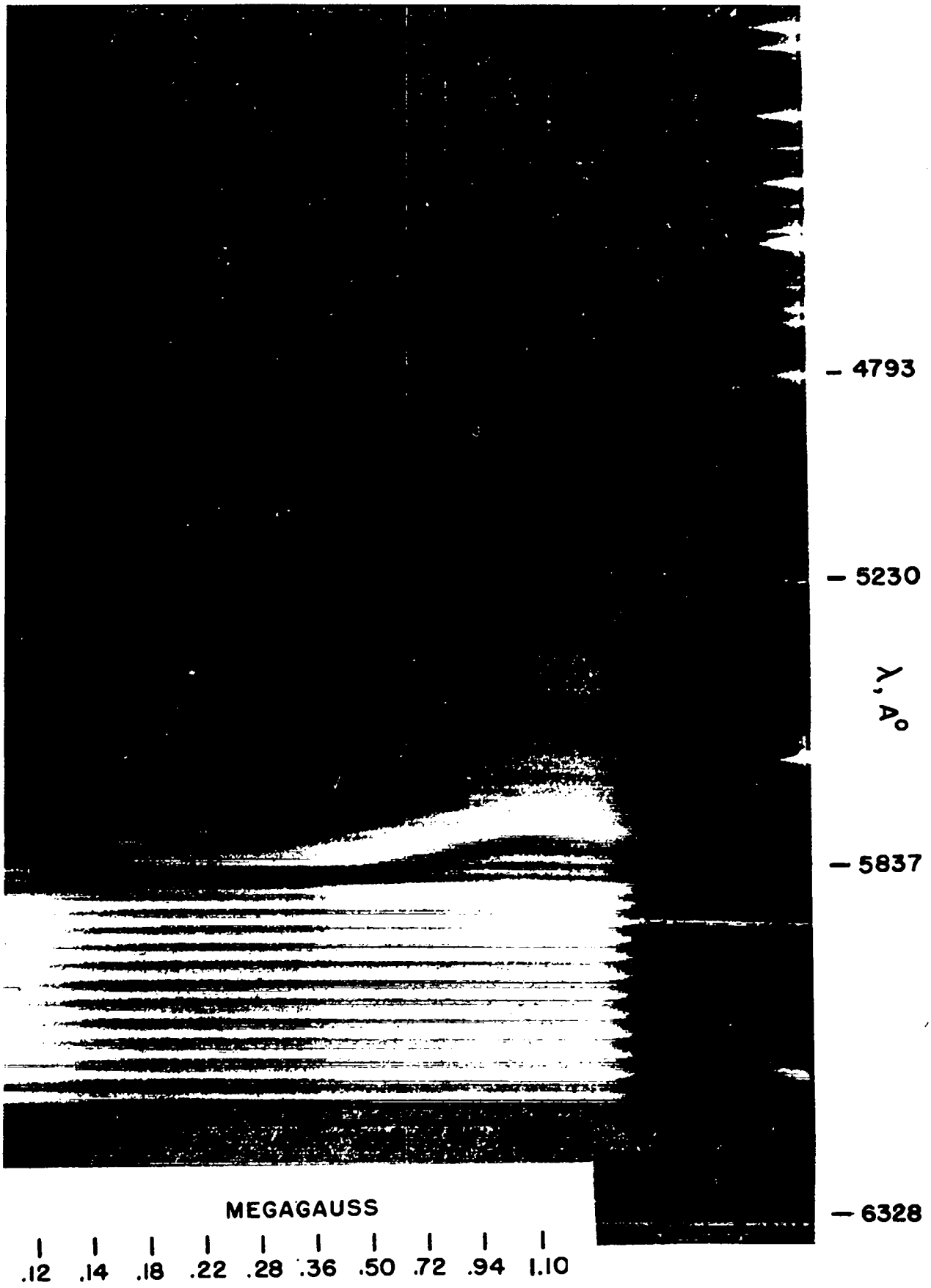

Figure 1.

Figure 2. Variation of GaSe Absorption Line Energies in cm^{-1} With Magnetic Field at 6.5°K.

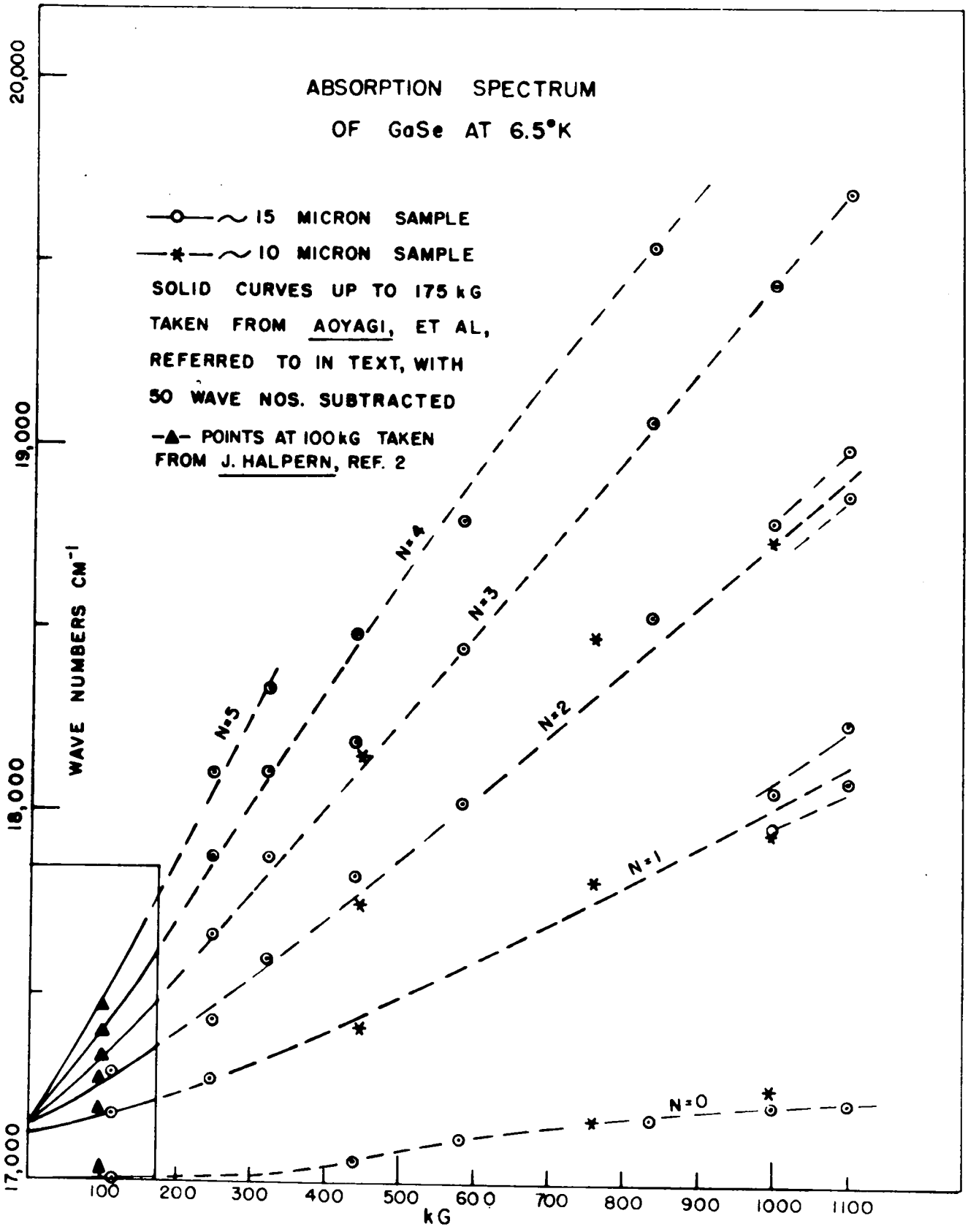
ABSORPTION SPECTRUM
OF GaSe AT 6.5°K
—o— ~ 15 MICRON SAMPLE
—*— ~ 10 MICRON SAMPLE
SOLID CURVES UP TO 175 kG
TAKEN FROM AOYAGI, ET AL,
REFERRED TO IN TEXT, WITH
50 WAVE NOS. SUBTRACTED
—▲— POINTS AT 100 kG TAKEN
FROM J. HALPERN, REF. 2
WAVE NUMBERS CM⁻¹
20,000
19,000
18,000
17,000
N=5
N=4
N=3
N=2
N=1
N=0
100
200
300
400
500
600
700
800
900
1000
1100
kG

Figure 2.

Excerpted from

Los Alamos Scientific Laboratory

Internal Document GMX-6-789,

June 1971

Solid State Experiments - W. B. Garn, R. S. Caird, and C. M. Fowler

The spectrographic investigation of transparent crystals in a cryogenic (6.5°K) and high field environment is continuing. Additional shots have been fired using crystal samples of MnF_2, CdS, ZnS, ZnO and GaSe with the magnetic field increased to about 1.6 to 2 MG. These data supplement previous information obtained in the 1 MG region.

The Faraday effect (magneto optic rotation) for ZnO at 6.5°K behaved normally up to a 1.7 MG field (maximum field obtained during the shot). A plot of degrees rotation of the plane of polarization of the transmitted polarized light against magnetic field for a fixed wavelength (Fig. 1) yields straight lines. This shows that the Verdet coefficient is indeed constant for this range of fields. Any number of wavelengths can be plotted in this manner, limited only by the wavelength range covered on the original record. Figure 2 is a plot of Verdet constant versus wavelength for ZnO. These data, taken from the 1.7 MG shot, match earlier data from 1 MG shots. The spectrographic record is reproduced as Fig. 3. Wavelength calibration is obtained from a 6328 Å reference laser line on the right and a gold bridge wire spectrum at the top. Time increases towards the bridge wire spectrum (top) with the record terminating at about peak field.

A 1.7 MG shot, incorporating a ZnS sample, gave Faraday data that agreed with 1 MG data up to about 1 MG but for higher fields gave anomalous information. The plot of degrees rotation against field for this material remains straight up to about 1 MG and then for higher fields starts to curve. Figure 4 shows these curves for a few selected wavelengths. If this curvature is indeed real, the Verdet coefficient for this material has ceased to be a constant. The shape of the field record (Fig. 5) near the peak field time appears abnormal. Although unlikely, this difference may indicate a change in the sample

conductivity with a subsequent perturbation of the flux. A change of this nature would render both the field record and the spectrogram (Fig. 6) uninterpretable in this field region. Other possibilities include physical damage or movement of the probe. New assemblies with the field probe moved from around the sample to a new location will permit better protection of the probe and allow the field to be measured without being influenced by changes in the sample. Additional shots will be fired to resolve this anomaly.

CdS differs from the other crystals in that it exhibits an absorption edge in the visible region of the spectrum. Figure 7 is a reproduction of a 1 MG Faraday spectrogram of this material. The optical rotation versus B field plot for this material (Fig. 8) shows a pronounced curvature for wavelengths approaching the absorption edge even for modest fields below 1 MG. A 1.8 MG experiment with this same material indicated nonlinearity for all visible wavelengths at the higher fields above 1 MG (Fig. 9). The original spectrogram (1.8 MG) is reproduced as Fig. 10. Here again additional shots are needed to verify this anomaly. A 1.9 MG shot using a CdS crystal but without the polarizer and analyzer, and illuminated by an argon flash, gave the transmission spectrum illustrated in Fig. 11. At the peak field of 1.9 MG, the absorption edge has shifted towards the blue by about 63 Å.

A transmission spectrogram for MnF_2 taken for fields up to 1.94 MG (Fig. 12) exhibits very little structure above about 1 MG. This record duplicates data obtained from a previous 1.1 MG shot. The molecular field model predicts that as the field increases, the magnetic moments of the sublattices should tilt toward the field direction. The alignment should be complete at 1.1 MG. Two additional 1 MG shots were fired using different sample lengths

to try to bring out various components of the absorption structure but both experiments failed.

An attempt to extend the absorption spectrum of GaSe at 6.5°K up to the 2 MG region has been partially successful. Because of very weak records, usable data were obtained only for the N = 0 and N = 1 absorption lines. A very weak line appears to split off from the N = 1 line and has been labeled N = 1^1. These data are plotted as Fig. 13. Additional shots will be fired using this material as soon as a recently acquired image-intensifier tube has been installed on the Model 40 spectrograph. The intensified records should permit resolution of the higher quantum level lines (N = 2---5).

Mounting hardware have been fabricated to permit attaching the intensifier tube to the Model 40 spectrograph so this unit should be operational soon. Hopefully this tube will eliminate the weak photographic record problem which has plagued the spectrographic work.

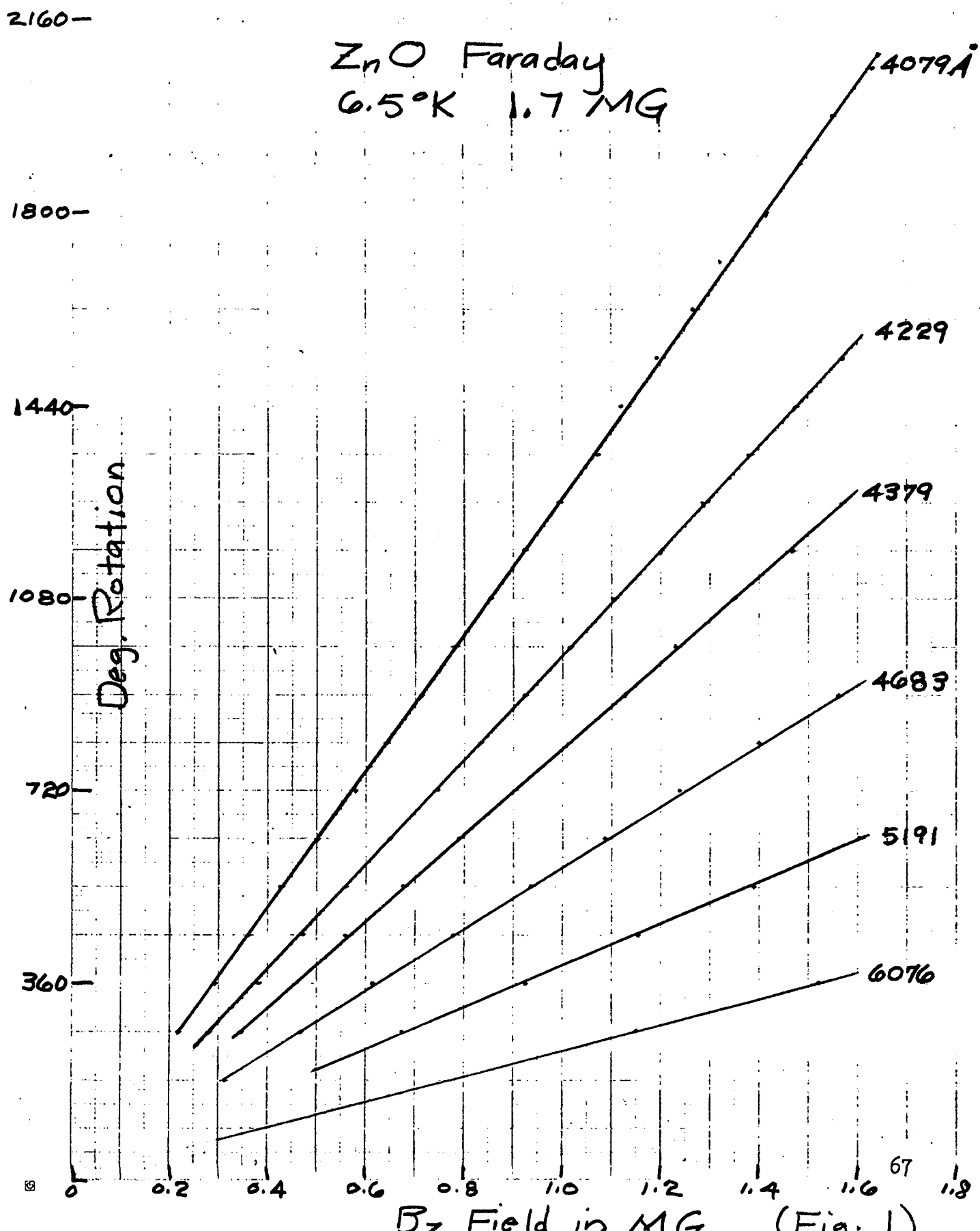
ZnO Faraday
6.5°K 1.7 MG
4079Å
4229
4379
4683
5191
6076
2160
1800
1440
1080
720
360
0
Deg. Rotation
0.2
0.4
0.6
0.8
1.0
1.2
1.4
1.6
1.8
Bz Field in MG

(Fig. 1)

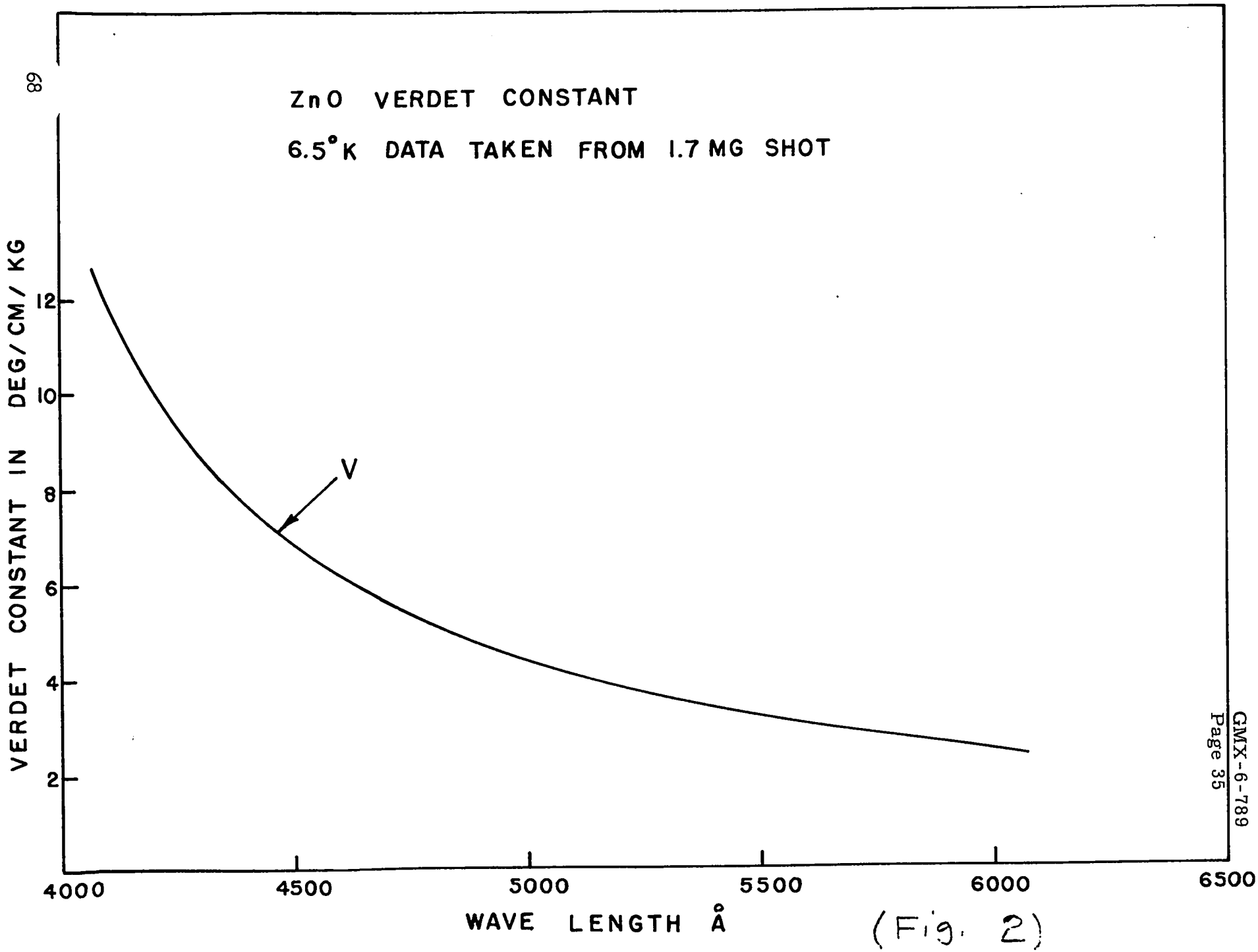
ZnO VERDET CONSTANT
6.5°K DATA TAKEN FROM 1.7 MG SHOT
VERDET CONSTANT IN DEG/CM/KG
12
10
8
6
4
2
V
4000
4500
5000
5500
6000
6500
WAVE LENGTH Å

(Fig. 2)

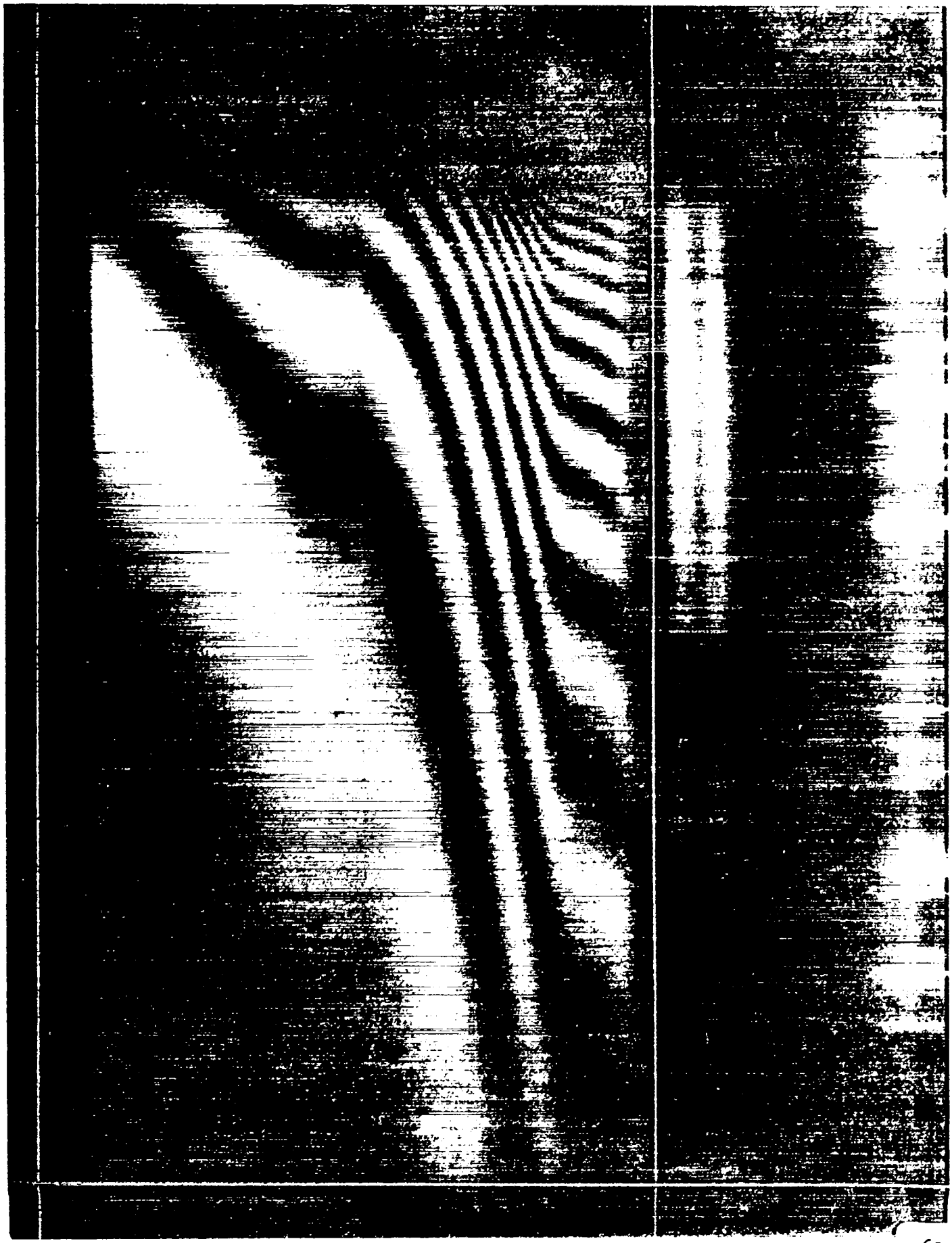

69

Figure 3

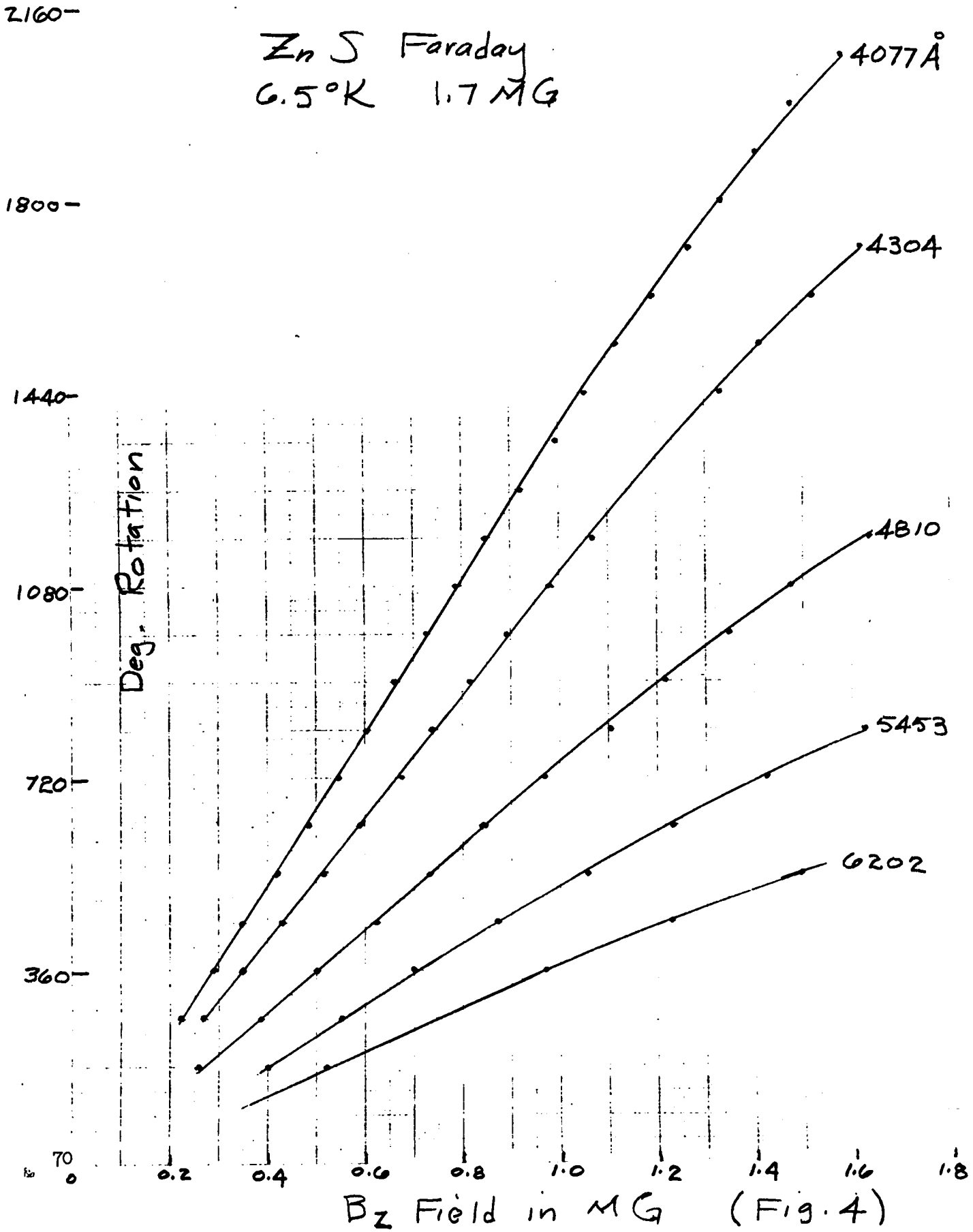
ZnS Faraday
6.5°K 1.7 MG
4077Å
4304
4810
5453
6202
2160
1800
1440
1080
720
360
70
Deg. Rotation
0
0.2
0.4
0.6
0.8
1.0
1.2
1.4
1.6
1.8
Bz Field in MG (Fig. 4)

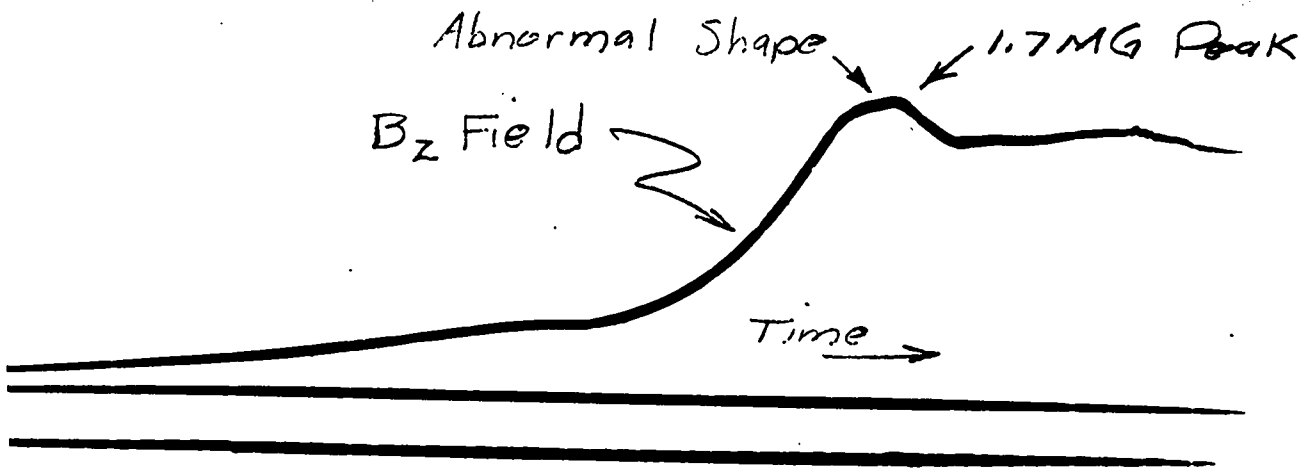

Figure 5

72

Figure 6

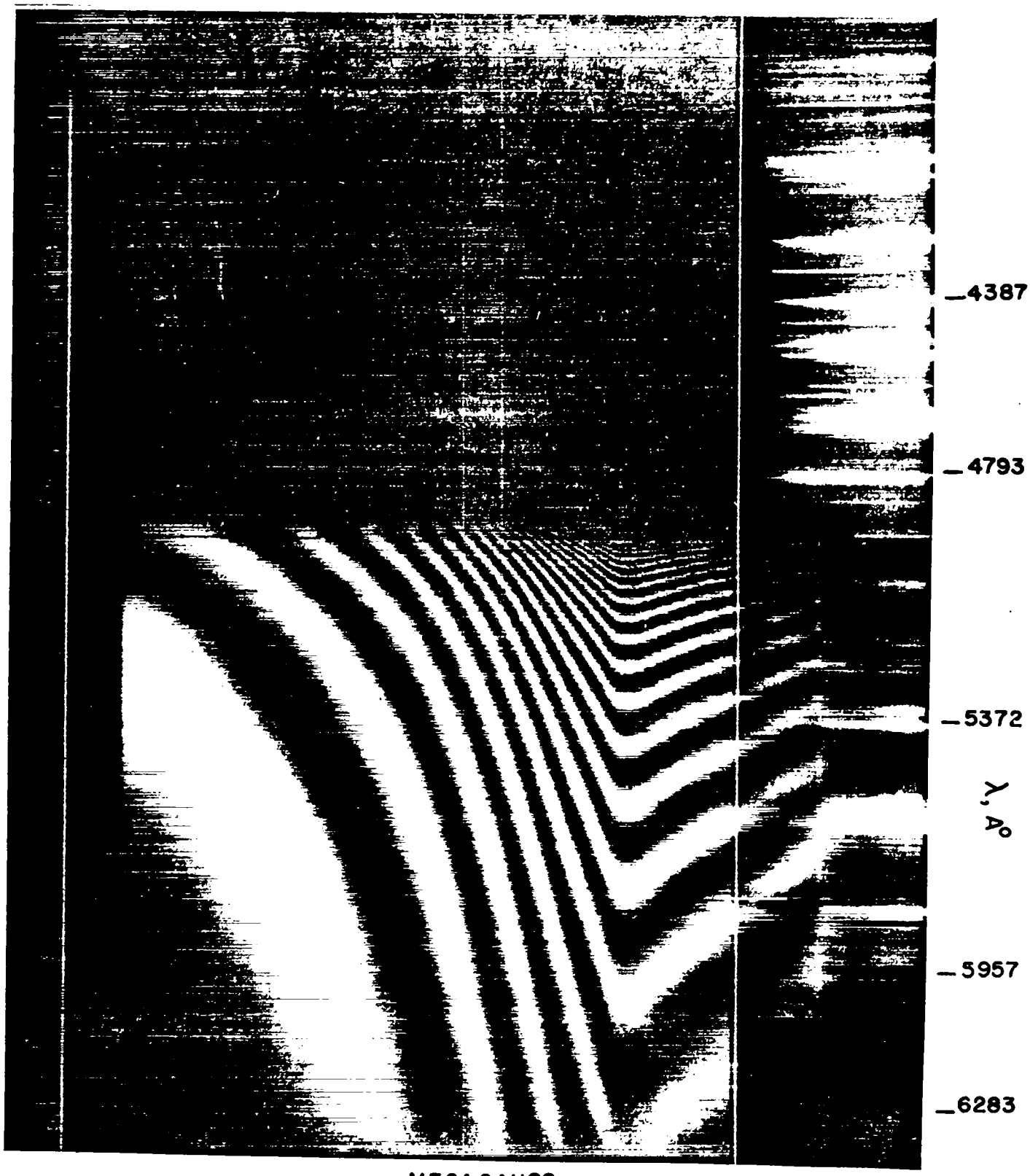
4387
4793
5372
5957
6283
λ, Å
MEGAGAUSS
.13
.18
.25
.41
.58
.81
1.0
.94

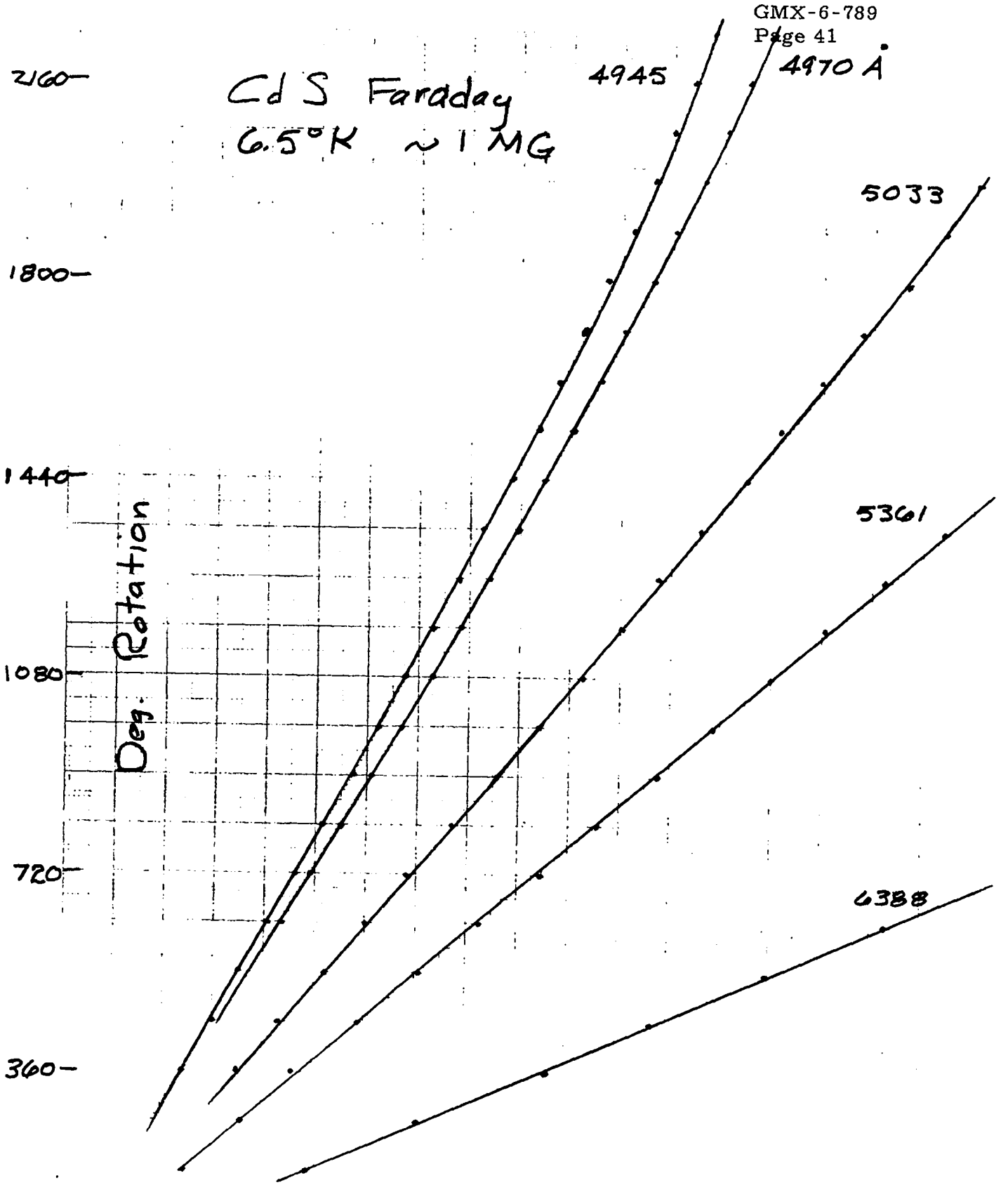
CdS Faraday
6.5°K ~ 1 MG
4945
4970 Å
5033
5361
6388
2160
1800
1440
1080
720
360
Deg. Rotation
0
0.1
0.2
0.3
0.4
0.5
0.6
0.7
0.8
0.9
Bz Field in MG

(Fig. 8)

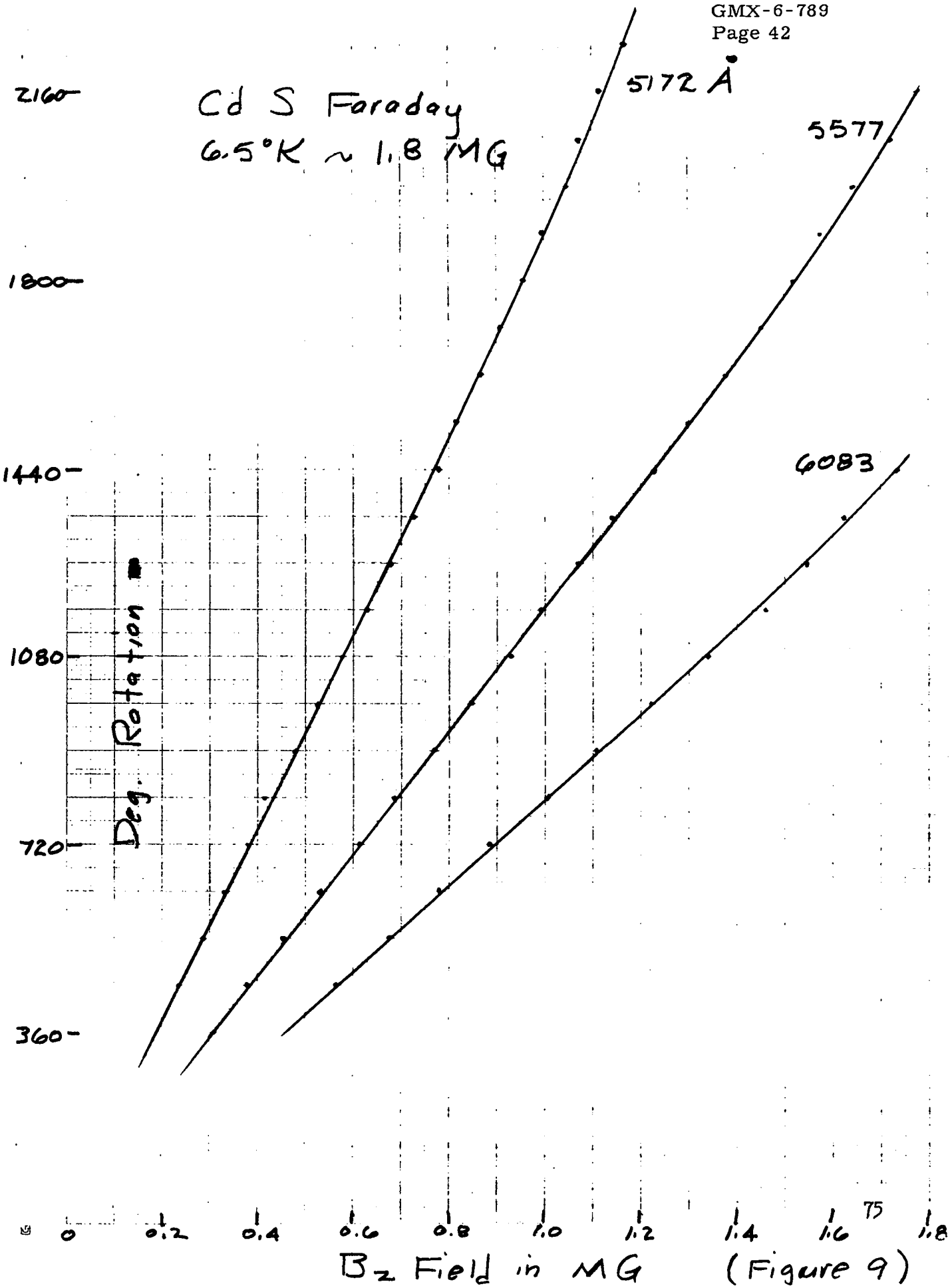
Cd S Faraday
6.5°K ~ 1.8 MG
5172 Å
5577
6083
2160
1800
1440
1080
720
360
Deg. Rotation
0
0.2
0.4
0.6
0.8
1.0
1.2
1.4
1.6
1.8
B_z Field in MG

(Figure 9)

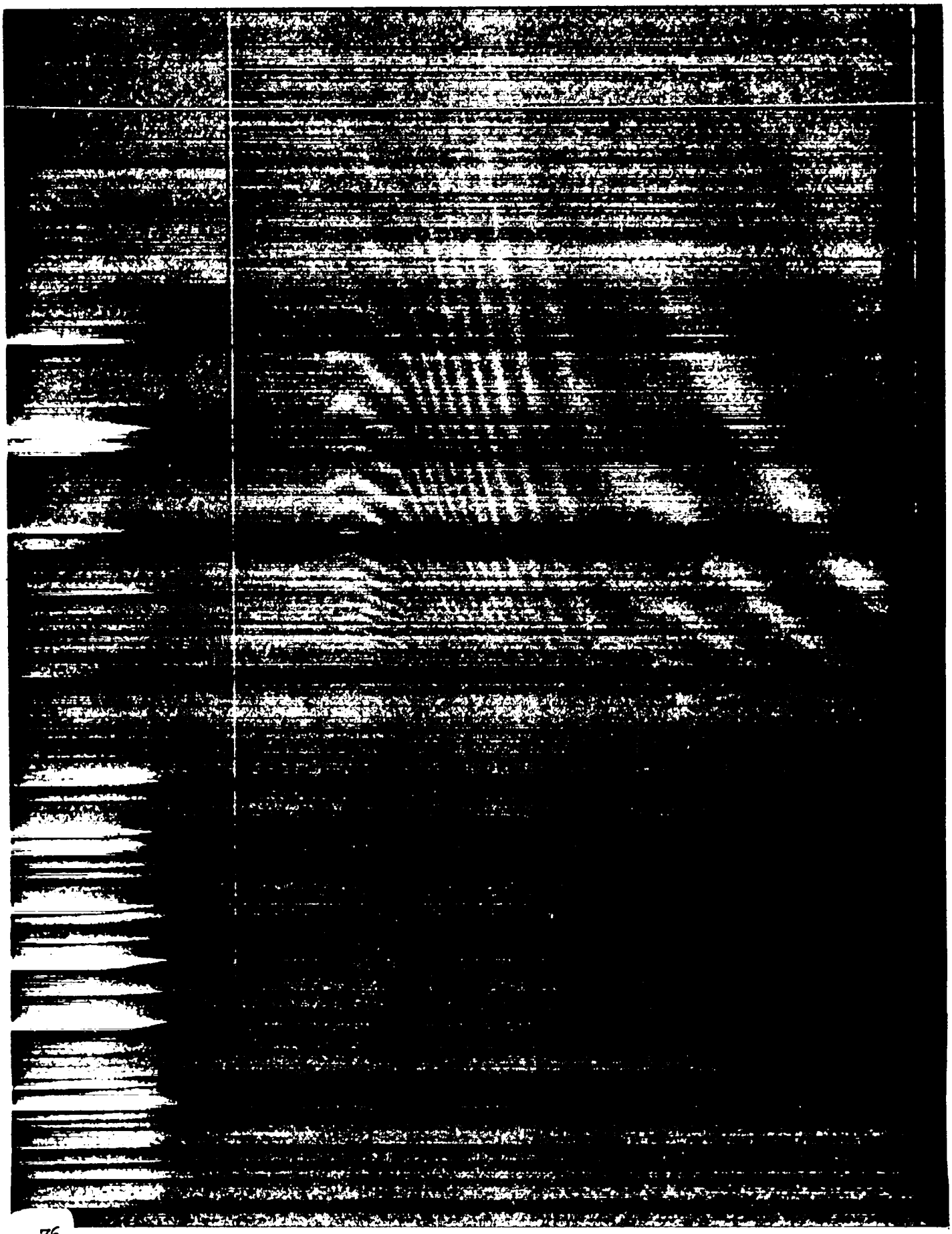

76

Figure 10

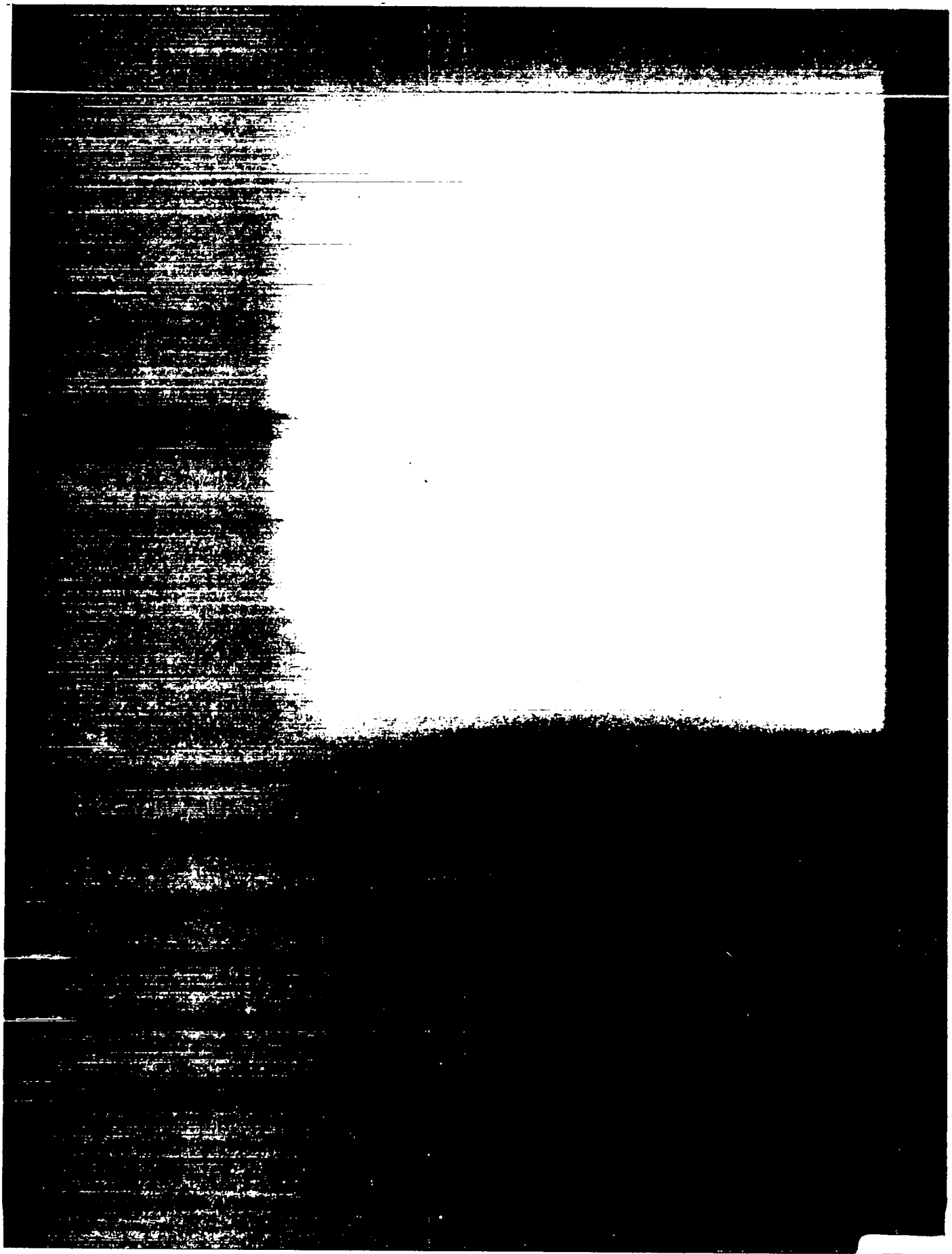

Figure 11

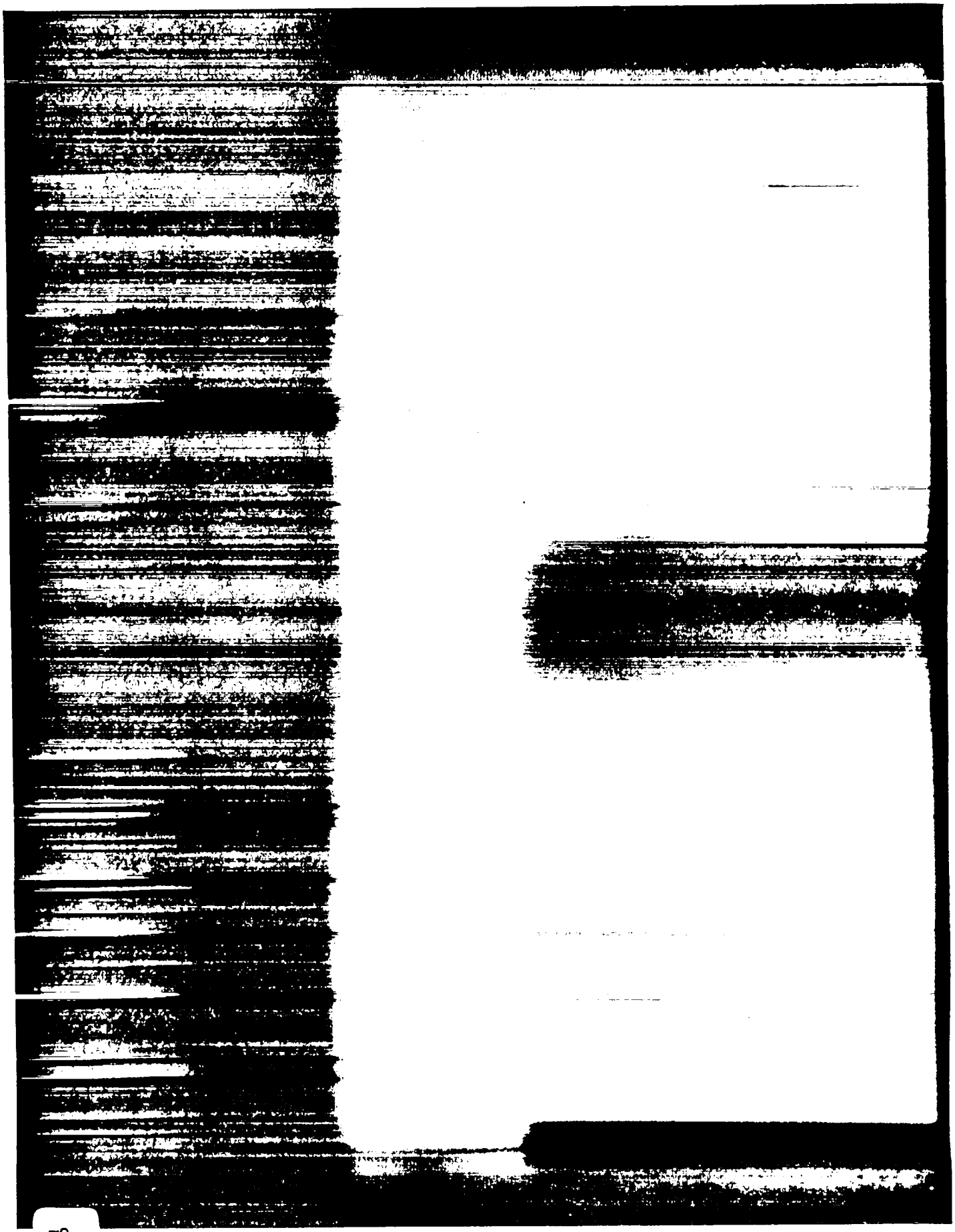

Figure 12

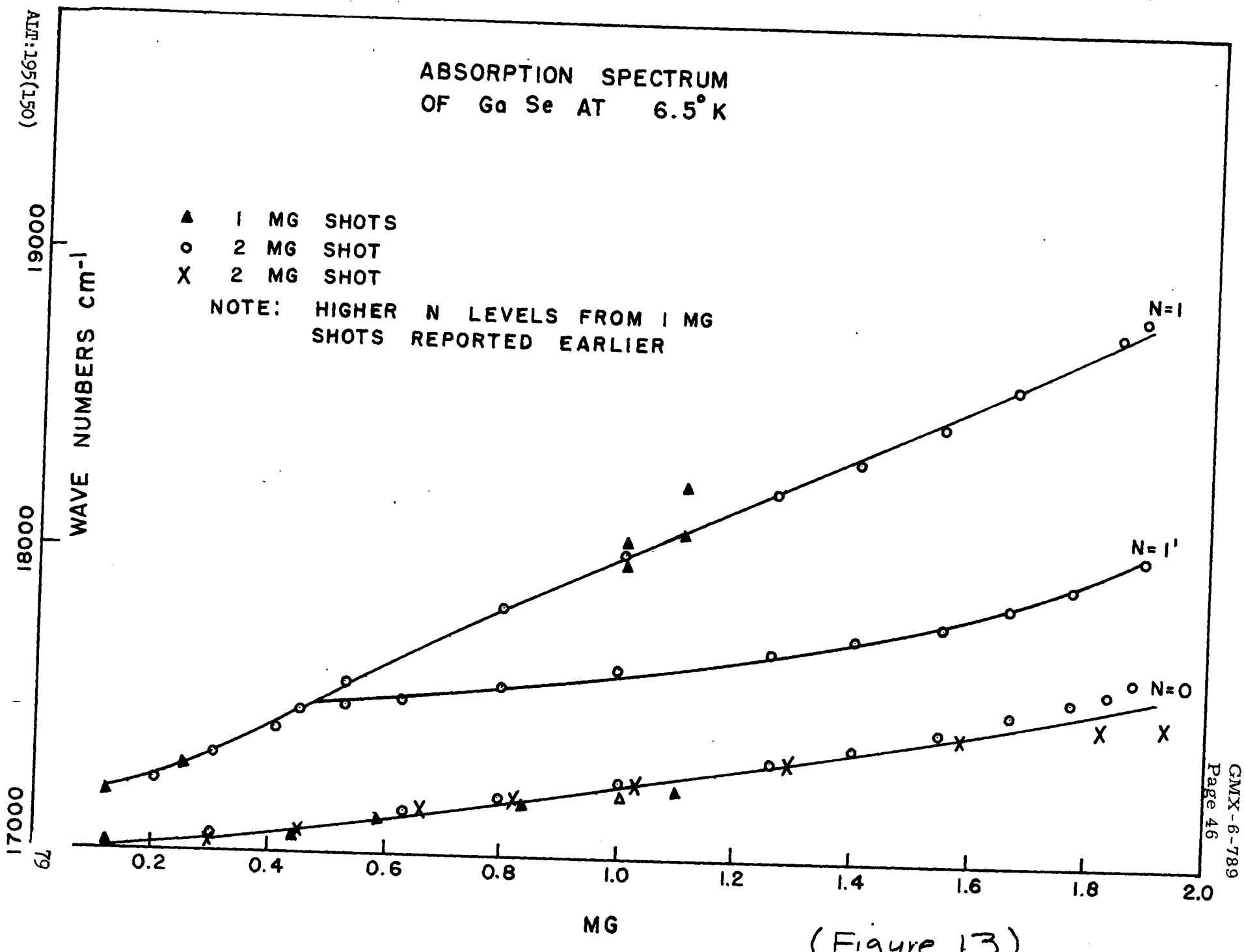
ALT:195(150)
ABSORPTION SPECTRUM
OF Ga Se AT 6.5°K
▲ 1 MG SHOTS
o 2 MG SHOT
X 2 MG SHOT
NOTE: HIGHER N LEVELS FROM 1 MG SHOTS REPORTED EARLIER
WAVE NUMBERS cm⁻¹
19000
18000
17000
N=1
N=1'
N=0
0.2
0.4
0.6
0.8
1.0
1.2
1.4
1.6
1.8
2.0
MG
79
GMX-6-789
Page 46

(Figure 13)